A Comparative study of the mineral composition of Macrotermes and Cubitermes termite mounds in Lualaba, D.R. Congo: Contribution to strategic prospecting for Cu and Co deposits

Serge Ilunga Ngoy, Yannick y Callec, Denis Thieblemont, Dona Kampata, Jean Félix Mupande, Apolline Auclerc, Françoise Watteau

▶ **To cite this version:**

Serge Ilunga Ngoy, Yannick y Callec, Denis Thieblemont, Dona Kampata, Jean Félix Mupande, et al.. A Comparative study of the mineral composition of Macrotermes and Cubitermes termite mounds in Lualaba, D.R. Congo: Contribution to strategic prospecting for Cu and Co deposits. Journal of Geochemical Exploration, 2022, 235, pp.106960. 10.1016/j.gexplo.2022.106960 . hal-03669499

HAL Id: hal-03669499

https://brgm.hal.science/hal-03669499v1

Submitted on 22 Jul 2024

HAL is a multi-disciplinary open access archive for the deposit and dissemination of scientific research documents, whether they are published or not. The documents may come from teaching and research institutions in France or abroad, or from public or private research centers.

L'archive ouverte pluridisciplinaire **HAL**, est destinée au dépôt et à la diffusion de documents scientifiques de niveau recherche, publiés ou non, émanant des établissements d'enseignement et de recherche français ou étrangers, des laboratoires publics ou privés.

Distributed under a Creative Commons Attribution - NonCommercial 4.0 International License

Version of Record: https://www.sciencedirect.com/science/article/pii/S0375674222000188
Manuscript_608c7bcebc490c5d314824d52121a005

A Comparative study of the mineral composition of *Macrotermes* and *Cubitermes* termite mounds in Lualaba, D.R. Congo: contribution to strategic prospecting for Cu and Co deposits

Serge Ilunga Ngoy[1], Yannick Callec[2], Denis Thieblemont[2], Dona Kampata[3], Jean Félix Mupande[4], Apolline Auclerc[1], Françoise Watteau[1]

1 : Université de Lorraine, INRAE, LSE, F-54000 Nancy, France

2 : Bureau de Recherches Géologiques et Minières, 3 avenue Claude Guillemin, BP 36009, F-45060 Orléans, Cédex2, France

3 : Service Géologique National C°/ Gombe, Kinshasa, DR Congo

4 : Cadastre Minier C°/ Gombe, Kinshasa, DR Congo

Corresponding author at: Laboratoire Sols et Environnement LSE/UMR 1120 INRAE – UL
2 avenue de la forêt de Haye BP 20163 54505 Vandoeuvre lès Nancy cedex France
Email : serge.ilunga-ngoy@univ-lorraine.fr (Serge Ilunga Ngoy)

Abstract

This work focuses on the comparative analysis of the influence of two termites of the *Macrotermes* (fungus-growing) and *Cubitermes* (soil-feeding termites) genera on the dynamics of soil lithogeochemical facies. The aim was to establish a general systematic recognition of the lithology of a large area, including its potential for Cu and Co mineralization. Eighty-eight samples of the mound material were collected from termite mounds of these two species along a 50 km transect in Lualaba Province, Democratic Republic of Congo (DRC) in order to carry out major and trace element analyses. Interpretation of the data was carried out through exploratory analysis, using the Ascending Hierarchical Classification (AHC) method and Principal Component Analysis (PCA), followed by statistical modeling using linear regression. After clustering the termite mounds into classes by AHC, an initial PCA was used to map the

© 2022 published by Elsevier. This manuscript is made available under the CC BY NC user license
https://creativecommons.org/licenses/by-nc/4.0/

lithology of these classes using major elements. The results highlight the dependance of the lithological composition of the mounds on the behavior specific to each of the two termite species. Linear regression modeling allowed a delineation of the area of supply of building materials for each species, indicating the possible incorporation of Cu and Co mineralizations likely to be present in the environment of the termite mounds. The use of termite mounds as a tool in mining exploration is discussed.

Keywords : Termites, Chemical composition, Major elements, Trace elements, Cu and Co mineralization, Katanga Supergroup.

1. Introduction

Termites are key contributors to pedogenic processes and the bioturbation of soil particles covering the bedrock (Stewart and Anand, 2014). Termites are amongst the main macroinvertebrate decomposers of organic matter in arid and semi-arid environments, exerting additional impacts through the creation of biostructures (mounds, galleries, sheetings, etc…) with different soil physical and chemical properties (Jouquet et al., 2011; Garnier-Sillam et al., 1991). Bachelier (1978) showed that the material in large termite mounds comes from deep soil horizons. All the authors acknowledge that these spectacular elevations also have an effect on the chemical enrichment of soils.

Many studies have highlighted this chemical and/or mineral enrichment of termite mounds in mineral clay, organic matter, major elements, trace elements and rare earths (Garnier-Sillam, 1987; Jouquet et al., 2004, 2007; Sako et al., 2009; Mujinya et al., 2013). Few of them have sought to exploit this information in mineral prospecting, some works have used this factor to highlight mineral occurrences in gold deposits (Roquin et al., 1991; Arhin and Nude, 2010; Gleeson and Poulin, 1989; Stewart et al., 2012; Stewart and Anand, 2014) or in locating uranium mineralization (Le Roux et al., 1991). Beyond these prospected metals, Sako et al.

(2009) argue that certain clays and organic matter have a selective affinity for trace elements found in termite mounds, such as Cd, Co, Cu, Ni and Zn. This assertion makes termite mounds a potential resource in tactical prospection for identification of polymetallic deposits. Systematic research has already been carried out in this context by Arveti et al. (2012) to compare the distribution of the chemical elements Cu, Pb, Zn, Ni, Co, Cr, Li, Rb, Sr, Ba and U in termite mounds and adjacent surface soils in mineral prospecting. However, no studies have focused on the geochemistry of termite mounds for strategic prospecting of vast regions.

In the landscape of the metallogenic province of Lualaba, one of the four provinces resulting from the dememberment of Katanga, two species of termites build their nests; the *Macrotermes* and *Cubitermes*. *Macrotermes*, a fungus-growing species, builds nests containing chambers for dead plant material such as wood, bark and straw, and arranges them in millstone patterns (Jouquet et al., 2007, 2011; Garnier-Sillam, 1987). This species breaks down dead plant material indirectly by growing fungi in galleries. The spatial distribution of these termite mounds in Katanga is estimated at 3 to 5/ha in the savanna and forest areas and these mounds are about 8 m high and 15 m wide (Mujinya et al., 2011). *Cubitermes*, a soil-feeding or humivorous termite species, builds termite mounds in the form of fungus with one or more caps (Grassé, 1950). The mounds of these humivorous termites are built with materials mainly originating from the surface horizon and recycled at this level by erosion. In contrast, the fungus-growing *Macrotermitinae* can retrieve their material (wet soil particles) from very deep down in the profile, even as far as the water table (Jouquet et al., 2011). These differences between termite mounds are species-dependent and due to genetic factors regulating the behaviour of workers (Grassé et al., 1961). Thus, exploiting the termite mounds in a region such as Katanga, which abounds in significant Cu and Co reserves (Kaya Muyumba et al., 2015), would constitute an alternative tool to traditional techniques in strategic and tactical geochemical prospecting. Strategic prospection is a method that leads to the systematic general

reconnaissance of a vast region. It highlights anomalous areas with a probable relationship to mineralization. Tactical prospection is applied to a specific occurrence with the aim to define detailed problems (deposit extension or mineralized structures on surface and at depth, etc.) (Granier, 1962).

The province of Lualaba is a major province of the Katanga copperbelt, with some of the richest Cu and Co deposits present in the Kolwesi area (Kamoto, Mashamba-East, KOV (Kamoto-East, Oliveira, Virgule), Musonoi, Kananga, Tilwezembe, Kalongwe...) (Cailteux et al., 2005; El Desouky et al., 2010) and the recently discovered Kamoa giant deposit (759 Mt at 2.57 wt% Cu) (Twite et al., 2019) located approximately 25 kilometers west of this town (Wendorff 2011, Twite et al., 2019).

This study focuses on the geochemical characterization and mapping of termite mounds of two major species in Katanga: *Macrotermes* and *Cubitermes*. This characterization led to the identification of behavioral differences between species, factors that influence the chemical composition of termite mounds. These differences were consolidated by predictive modeling of Cu and Co mineralization in the termite mounds.

2. Geological setting

The study area is located in the southeastern part of the Democratic Republic of Congo (DRC) in the Lualaba Province between 11°00' and 11°50' South latitude, and 24°50' and 25°00' East longitude on the Kayoyo Sheet (Fig.1). This area is located in the north-western part of the Katanga copperbelt, a Neoproterozoic orogenic belt forming a north-directed thrust-and-fold belt, called the “Lufilian Arc”, located between the Congo and Kalahari cratons. It is more than 150 km wide and stretches for 700 km from Mwinilunga in the west, to Kolwezi in the

105 northwest, up to Luanshya (previously Roan Antelope) and Lonshi in the southeast (Cailteux
106 et al., 2005; Batumike et al., 2007; Cailteux and De Putter, 2019; Twite et al., 2019).
107 The neoproterozoic terrains of the Katanga Copperbelt are commonly interpreted as a 7.5-10
108 km thick sedimentary deposits developed in a ~880 Ma rifted intracontinental basin, between
109 the Kalahari and Congo cratons, which occurred during the Rodinia Supercontinent break-up
110 (Armstrong et al., 2005). This succession was affected by the ~573-530 Ma Lufilian orogeny,
111 linked to the amalgamation of the Gondwana Supercontinent and the convergence between the
112 two cratons. It developed a fold-and-thrust-belt to the north detaching the Katanga sedimentary
113 sucession from the Bangweulu Paleoproterozoic basement (Kampunzu and Cailteux, 1999,
114 Kipata et al., 2016). The Lufilian belt differs in deformation style and metamorphic grades from
115 the south to the north with respectively: the Dome region exposed in Zambia and the Lufilian
116 arc (composed of an internal highly-structured domain and an external domain including the
117 Kamoa sub-basin) and the tabular Kundelungu domain. For the Lufilian arc domains, the formal
118 stratigraphy was described by François (1974) and has been recently revised by Cailteux et De
119 Putter (2019), the latter version being used in this paper. In the external Lufilian domain, the
120 lithostratigraphy of the Katanga succession is subdivided into three groups from bottom to top:
121 (1) A carbonate sequence of the Roan Group (R); (2) A dominant silicoclastic sequence of the
122 Nguba Group (Ng); (3) a mixed-terrigenous and carbonate succession of the Kundelungu Group
123 (Ku). These groups are separated by stratigraphic unconformities based on the presence of two
124 regional diamictites considered as stratigraphic markers, known as the “Grand-Conglomerat”,
125 or the “Mwale sub-group” and the “Petit Conglomérat” or the “Kyandamu sub-group”
126 (François, 1974; Batumike et al., 2007; Cailteux et al., 2019; Delpomdor et al., 2020). The two
127 regional diamictites represent two worldwide glacial events during the Neoproterozoic era. The
128 older diamictite, Grand Conglomérat (~720 Ma) can be correlated with the Sturtian glaciation

and the younger, Petit Conglomérat or Kyandamu Formation (~635 Ma) can be correlated with the Marinoan glaciation (Mambwe et al., 2017).

As illustrated by Fig. 2, the sampling transect was selected to cross part of the external Lufilian arc with two subdomains: (1) The northern autochtoneous subdomain, part of the Kamoa sub-basin with Kudenlungu deposits preserved in a NE-SW syncline and (2) the southern parautochtoneous subdomain affected by thrusts to the north and narrow NE-SW folds mostly affecting the Nguba series. Late oblic faults (NNE-SSW and NW-SE) create offsets in the folds and thrusts where the Roan Group outcrop with frequent breccia to megabreccia facies (Cailteux et al., 2018).

Table 1 presents a detailed and revised lithostratigraphy of the Katanga Supergroup, exposed in the study area, mainly based on drillhole descriptions including a lithological description of each unit. In the field, due to poor outcrop conditions, geological mapping fails to be as precise and some of the mapped geological units designated as "undifferentiated" have a composite lithostratigraphical and lithological description.

From a metallogenic point of view (e.g. Cailteux et al., 2005), the Katanga Copperbelt is one of the world's greatest copper-cobalt province, representing more than half of the world's mineable cobalt and the second largest global reserve of copper. Cu and Co are closely associated in many deposits generally in the form of disseminated sulphides forming stratiform orebodies hosted in fine-grained siliciclastic, black shales or dolomitic sedimentary rocks, and thought to have resulted from syngenetic and early diagenetic processes. During the panafrican orogeny, they are also remobilized (i.e. tectonic breccia) along the main thrusts and secondary faults (Decree et al., 2014). No evidence exists that metals could have originated from Katangan igneous through hydrothermal processes. Association of copper and cobalt with iron, and sometimes with anomalous concentrations of other metals (e.g. Ni, U, Cr, Ag, Au, PGE) led

Cailteux et al. (2005) to suggest that Katangan deposits could have resulted from the remobilization of low-grade Cu-Co deposits present in the pre-Katangan basement.

3. Materials and methods

3.1. Termite mound sampling strategy

In a landscape dominated by a mosaic of natural miombo-type open forest ecosystems, characterized by the dominance of species of the genus *Brachystegia* that grow in semi-arid areas of the tropical savannah (Malaisse, 2018), eighty-eight (88) termite mound samples, including 60 *Macrotermes* termite mounds and 28 *Cubitermes* termite mounds, were collected along a ~ 50 km transect from the village of Musokatanda to the Zambia-DRC border southwest of Lualaba beyond the village of Ikekeketi. This transect crosses three geological formations as described above (Fig. 2).

Samples from *Macrotermes* termite mounds were collected from the central point between the top and base of each termite mound and samples from *Cubitermes* termite mounds were collected from the top of each termite mound in order to avoid any contamination of the mound material by the underlying soil. All samples were taken after scraping away the first layer of the termite mound. The sampling revealed that *Cubitermes* termite mounds are monochrome (gray) and ~ 30 cm high, as opposed to *Macrotermes* termite mounds which are polychrome (grey, beige, yellow, brown, red) (Fig. 3) and varied in size whose height ranges from 1.7 to 9 m with an average of 5.16 m (Fig. A.1).

Figure 4 illustrates the color contrast of *Macrotermes* termite mounds. Termite mounds on Kalahari sands and Kundelungu Group formations are predominantly gray and beige, while those on Nguba Group formations are predominantly yellow, red and brown. Most of the red and brown termite mounds are located on the Mwale subgroup.

3.2. Analysis of samples and statistical methods

After drying, crushing and sieving to fractions of 160 µm, the termite mound samples were deposited at the regional branch of ALS-Minerals laboratory in Lubumbashi in the province of Haut-Katanga to be sent to the laboratory in Vancouver, Canada for multi-element analysis. All samples were analyzed using the ICP-AES / ICP-MS multi-element acid digestion method to determine 48 elements, namely: Ag, Al, As, Ba, Be, Bi, Ca, Cd, Ce, Co, Cr, Cs, Cu, Fe, Ga, Ge, Hf, In, K, La, Li, Mg, Mn, Mo, Na, Nb, Ni, P, Pb, Rb, Re, S, Sb, Sc, Se, Sn, Sr, Ta, Te, Th, Ti, Tl, U, V, W, Y, Zn, Zr. These analyses have followed quality control procedures based on 3 types of QA/QC samples: (1) blanks (multicentimetric to decimetric geodic quartz vein crystals of gem quality collected northwest of Kolwezi); (2) standards (insertion of bags containing 60g of OREAS 45e[7] and OREAS 904[8] standards); (3) preparation duplicates (division of some samples in two during the preparation phase in order to control the stability of the analytical conditions and the sample preparation process). In order to allow the statistical processing of the data for values below the detection threshold, we proceeded with a classical geochemical processing approach, by which the values below the detection threshold of each element were replaced by half of it (Grunsky and Smee, 1999). Three elements were not taken into account in the statistical treatment (rhenium (Re), selenium (Se) and tellurium (Te)), as the majority of their values being below the detection limit, after applying this method, which meant the statistical software considered them as constants.

The termite mounds of each type were first separated into different classes by the method of Ascending Hierarchical Classification (AHC), and we were then able to establish a mineralogical profile of these classes by Principal Component Analysis (PCA) based on the major elements (Moradpouri and Mohammad, 2021, Sikakwe et al., 2020). After a comparison of the means of all the elements according to their abundance in the upper continental crust, the variables with significant mean concentrations were retained (As, Bi, Cs, Hf, Sb, Th, U, Zr) for

205 a second PCA in order to select variables capable of explaining the variability of Cu and Co in
206 the termite mounds using unconformities selt linear regression processes. All the statistical
207 analyses were implemented with XLSTAT Software 2020.
208
209
210 # 4. Results and discussion
211
212 ## 4.1. Geochemical characterization of termite mounds
213 Multivariate analysis using the AHC method applied both to major and trace elements was used
214 to determine the diversity of the geochemical composition of termite mounds. Fig. 4 shows the
215 dendrograms of the two sample sets. The AHC allowed eight (8) distinct classes to be
216 individualized for the series of *Macrotermes* termite mounds and five (5) classes to be
217 distinguished for the series of *Cubitermes* termite mounds (Fig. 5).
218 Table 2 groups together the means and standard deviations of the different classes defined by
219 AHC for each set of samples. After AHC, as Class 3 of the *Cubitermes* termite mound series
220 had only one sample, it was disqualified from further analysis.
221 Following the AHC treatment, an initial PCA was carried out in parallel with a correlation
222 analysis on the major elements analyzed (Al, Fe, Ca, Na, Mg, K, Ti) in order to determine the
223 elemental profile of each class and to compare it to that of the cartographic ensembles of the
224 study area. In both termite mound species, we found significant positively-correlated pairs
225 between Al and Ti, with $r = 0.7$, $p < 0.00$ for the *Macrotermes* termite mound series and $r = 0.6$,
226 $p < 0.00$ for the *Cubitermes* termite mound series and also Mg-K, Na-K, and Na-Mg pairs with
227 respectively $r = 0.6$; $r = 0.7$ and $r = 0.5$ for the *Macrotermes* termite mound series, and $r = 0.9$;
228 $r = 0.8$ and $r = 0.8$ for the *Cubitermes* termite mound series, all at $p < 0.00$. In the *Cubitermes*
229 termite mound series, there were also significant negative correlations between Ti and K, Mg
230 and Na, with respectively, $r = -0.6$, $p < 0.003$; $r = -0.5$, $p < 0.007$; $r = -0.6$, $p < 0.003$. In addition

to this point of divergence, in the *Macrotermes* termite series, there was a positive correlation between K and Fe, with $r = 0.3$, $p < 0.04$ and in the *Cubitermes* termite series, Na having a significant negative correlation with Al ($r = -0.4$, $p < 0.02$).

Fig. 6 represents the PCA of the two series carried out with these major elements. It can be seen that the distribution of classes based on the major elements makes it possible to distinguish characteristic associations between elements. In spite of differences in the background, we observe that the two series present two types of associations, one characterized by the variables Al and Ti and the other by K, Mg and Na. In the *Cubitermes* termite mound series, an intermediate association of classes was associated with the Fe variable carried by the F2 axis

The PCA of the *Macrotermes* separates Classes V, VII and VIII (mean Al contents: 9.62-11.14% and Ti between 0.81-0.98%) from Classes I and IV (mean Al contents: 6.90-7.90% and Ti: 0.35-0.44%). The F1 axis, which carries the variables K, Mg and Na, isolates Classes III and VI (average K contents: 1.13-1.25%; Mg: 0.27-0.32% and Na: 0.020-0.023%) from Classes II and IV (average K contents: 0.24-0.67%; Mg: 0.10-0.20% and Na: 0.013-0.016%). Of the 68.37% of variability explained by the PCA of the *Cubitermes* termite mound series, 48.32% of variability is explained by the F1 axis, which opposes classes with high Al and Ti contents to classes with high K, Mg and Na contents. Classes 1, 2 and 5 have average Al contents between 6.84-8.69% and average Ti contents between 0.62-0.73%. These three classes are opposed to Class 4 which has Al contents of 6.92% and Ti contents of 0.50%. The K, Mg and Na contents are much higher than these three other classes.

Due to their direct relationship to mineralogy, the major elements are representative of the nature of the rocks. In the hypothesis where the different classes would translate the differences between the rocky substrates of the sampling area, the termite mounds can then be used to determine the lithology of these substrates.

After conversion of major element contents (Table 2) to oxide percentages, we compared them to the average of the upper continental crust (UCC) of granitic composition estimated by Taylor and McLennan, 1985 (Table 3).

In the absence of either bedrock samples or lithological discontinuities in the soil horizons, the upper continental crust can be used as a surrogate for the source materials (Sako et al., 2009). Comparison of the major elements mean contents (expressed as oxides) with the means of the upper continental crust (UCC) indicates that in both series, the mean TiO_2 content is always higher than in the UCC. The same observation is made for mean Al_2O_3. In both series, CaO, K_2O, MgO and Na_2O contents are low compared to the mean contents in the upper continental crust. The *Macrotermes* termite series has a wide range of FeO contents and Class VI is the only one to have a mean content of 10.12%, which is much higher than that of the upper continental crust (FeO = 7.2%).

The average SiO_2 content of the upper continental crust is 66% (Taylor and McLennan, 1985). Among the major elements, only Al, Ca, Fe, K, Mg, Na and Ti were determined in the termite mound samples. With Si (and O), these are the main constituents of the upper continental crust representing more than 99% of the total (Taylor and McLennan, 1985). An approximate evaluation of the SiO_2 is given by difference between the sum of the analyzed oxides and 100% (Table 3). In all cases, this difference is lower than the mean SiO_2 content of UCC and this relative depletion increases as the Al_2O_3 content increases.

So, we can state that the main constituents of termite materials are SiO_2 and Al_2O_3, these materials also display an affinity for TiO_2 and sometimes FeO, depending on the termite mound location. An abundance of Si and Al can attest to a source material dominated by quartz and clays, such as sandstones, flints, clayey rocks or laterites. The low contents of Ca and Mg exclude any influence of carbonate rocks (limestones, dolomites...), thus suggesting non-incorporation by termites or more probably leaching of these elements in the materials used by

280 them. The low CaO, MgO and Na_2O contents and moderate K_2O contents (Table 3) suggest
281 that the termite materials are extracted from lateritic formations (Tardy, 1997) resulting from
282 the physico-chemical alteration of previous rocks without notable pedological transformations.
283 As illustrated by Figures A.2 and A.3, on the eight classes of the *Macrotermes* termite mound
284 series, five (III, IV, V, VI and VII) are located on the Mwale formation. The remaining series
285 are on the undifferentiated Nguba and Kundelungu terrains. The occurrence of contrasted
286 classes for a given formation may suggest that the termite mound materials are derived from
287 different mineralogical sources which are not discriminated by the 1/200 000 scale geological
288 map i.e. the formations defined as « undifferentiated ». In the case of the Mwale Formation,
289 whose thickness decreases from north to south from 1300 m in the Nzilo area to 120 m in the
290 Kyona area (Batumike et al., 2007), different units are defined, whose importance varies from
291 place to place. At Kamoa, for example, Twite et al. (2019) identified in Mwale six stratigraphic
292 units, while at Tenke Fungurume seven units were identified by Mambwe et al. (2017). The
293 mineralogical contrasts separating the classes present on this formation would be due to
294 lithological differences between these units, likely to provide varied sources for termite activity.
295 Beyond identifying chemical facies of the termite mounds, superposing the sample points of
296 *Macrotermes* termite mounds on the geological map reveals that these biostructures would be
297 good indicators of geological structures (faults and fissures) and the limits of the subjacent
298 formations. For example, a termite mound sampled on a fault has a different geochemical
299 signature to its two neighbors to the north and south on the sampling transect (Fig. 7). On the
300 other hand, a sample taken at the limit of a geological formation on the map signifies a
301 mineralogical composition other than that of the class that precedes it on the transect.
302 The *Macrotermes* termite mounds observed on the Nguba Group formations have very high Co
303 and Cu contents compared to the other termite mounds, except for the single gray termite mound
304 on Kalahari sand south of the transect that has the highest Co content of 19.6 ppm. On the

Nguba Group formations, the brown termite mounds have the highest Cu and Co contents, the richest of which is located on the Mwale Subgroup. Cu contents in the red, yellow and beige termite mounds on the Nguba Group formations are in the range of 15-200 ppm and Co contents vary from 2.8 to 12.7 ppm. Termite mounds on Kundelungu Group formations have the lowest Co (2.6-5.6 ppm) and termite mounds on Kalahari sand have the lowest Cu ranging from 14.6-29.1 ppm (Fig. 8).

4.2. Cu and Co availability prediction in termite mounds

From a comparison of the means of all trace elements (Table 2) with their abundance in the upper continental crust (Taylor and McLennan, 1985), eight (8) elements (As, Bi, Cs, Hf, Sb, Th, U, Zr) stand out from the others with very high average concentrations in almost all classes of the two series (Table 4).

These elements were retained for the continuation of the modeling process using multiple linear regression to explain the variability of Cu and Co in the termite mounds.

The principle of the linear regression method is to model a quantitative dependent variable Y, here Cu and Co, through a linear combination of p quantitative explanatory variables. The deterministic model is written for an observation n (Addinsoft, 2021): $\mathbf{Y = C_1X_1 + C_2X_2 + ... + C_nX_n + C_0}$, where Y is the dependent variable, X_n are explanatory variables, C_n are the weights of the X_n variables, and C_0 is the model constant.

In this study, we used a descending step-by-step regression that starts with all available variables, removing the least important at each step (Kouassi et al., 2014). A second exploratory analysis using the PCA method preceded this modelling process and made it possible to reduce the number of explicative variables in order to identify the most relevant variables capable of explaining the behavior of Cu and Co (Fig. 9). The PCA results for both series show that some of these eleven selected variables have significant correlations with Cu and Co. In the *Macrotermes* termite mound series (Fig. 9a), despite the low percentage of variability explained

by F3 (16.44%) compared to F2 (17.49%), this axis (F3) is the only one that clearly represents the Co variable with a value close to 1. The F1 axis associates the variable Cu with the variables Bi, Cs, Hf, Th, U and Zr, and F3 reflects a negative correlation between Co and Sb. In the *Cubitermes* termite mound series Cu and Co have a negative correlation with As and are all on the F1 axis. Thus, for the multiple regression modelling of the *Macrotermes* termite mound series, the variables Bi, Cs, Hf, Sb, Th, U and Zr were retained and for the *Cubitermes* termite mound series, the variables As, Cs and Th were retained.

After two stages of modeling, the multiple linear regression was transformed into a simple linear regression. The information provided by Sb for Co and Bi for Cu in the *Macrotermes* termite mound series and by Cs for Co and Th for Cu in the *Cubitermes* termite mound series, were found to be highly significant in explaining the variability of these two dependent variables at a chosen significance level of 5%. Table 5 gives details on the coefficient parameters of each model with 95% confidence intervals.

Among the four models, only the Co model in the *Macrotermes* termite mound series has a coefficient (model slope) with a negative value (variable Sb). This confirms the result of the PCA. This reflects an inversely proportional variation of the dependent variable with respect to the explicative variable (the diminution of Co with the augmentation of Sb). This model is also the only one to have a positive value for the constant. The standard errors give the percentages of the residuals that our models were unable to capture. From these coefficient parameters it is possible to derive a mathematical relationship of simple linear regression that links the dependent variables (Co and Cu) to the explicative variables. Thus, the equations of our models can be written as follows:

- For Co in the *Macrotermes* termite mound series : $\boldsymbol{Co = -2,794 * Sb + 8,200}$
- For Cu in the *Macrotermes* termite mound series : $\boldsymbol{Cu = 218,484 * Bi - 24,642}$
- For Co in the *Cubitermes* termite mound series : $\boldsymbol{Co = 0,897 * Cs - 0,096}$
- For Cu in the *Cubitermes* termite mound series : $\boldsymbol{Cu = 5,632 * Th - 41,961}$

Figure 10 illustrates the variability of Cu and Co concentrations in these four models. The values 0.519 and 0.410 of the determination coefficient R^2 for the *Cubitermes* termites mound series reflect the good fit of these two models to the data (Fig. 10c and 10d). In the two models obtained for the *Macrotermes* termite mound series, the data are scattered around the models, thus explaining the low values of R^2.

According to the Goldschmidt classification, the two explicative variables (Sb and Bi) for the *Macrotermes* termite series are chalcophilic elements, while those (Cs and Th) for the *Cubitermes* termite series are lithophilic elements. This classification is based on the affinity of lithophilic elements for oxygen and therefore aluminates and silicates and on the affinity of chalcophilic elements for sulfur and therefore sulfides. Thus the modellisation suggests that Cu and Co are in the sulfide form in the *Macrotermes* materials and in the oxidized form in the *Cubitermes* materials.

According to Fontaine et al. (2020), the mineralization processes of the Katanga Supergroup occurred in four episodes, the first three of which concern the mineralization of disseminated sulphides in thin beds, nodules or as vein/fracture in fine-grained siliciclastic and carbonate sedimentary rocks belonging to a unit known as the Mines Subgroup present in the lower part of the Roan group. The fourth episode exists in the alteration and oxidation of the preceding mineralization resulting in the formation of secondary ores located in the oxidized zone to a depth of 100 to 150 m (Kaya Muyumba et al., 2015; De Putter et al., 2016). Referring to the mineralization of the Katanga Supergroup, it is suggested that the *Macrotermes* species dig to a greater depth to construct their edifices, allowing them to bring up particles of unoxidized mineralization, whereas *Cubitermes* obtain material from superficial formations bearing oxidized mineralization.

Experiments by Jouquet et al. (2002) on termite mounds of *Odontotermes nr. Pauperans* (*Termitidae*, *Macrotermitinae*) reveal that termites obtain building materials from the deep soil.

382 The upper soil is used only when termites have no choice. The authors argue that termites
383 probably prefer to use the fine particles present in the deeper soil horizons rather than the
384 coarser materials marking the topsoil. In this study, the difference in material supply areas
385 between the two species may be due to different worker behaviours leading *Macrotermes*
386 (fungus-growing) to descend more deeply than *Cubitermes* (soil-feeding termites), the latter
387 supplying themselves with materials derived from superficial formations.
388
389
390 # 5. Conclusions
391
392 Analyses of samples of *Macrotermes* and *Cubitermes* termite mounds collected in Lualaba,
393 Democratic Republic of Congo, have shown that the major and trace elements they contain
394 have a lithological origin specific to the subjacent rock substrates. The termite mounds have
395 geochemical signatures that are likely to reflect the lithological domain of these substrates that
396 provide the termites with the materials necessary for the construction of their edifices. As such,
397 the termite mounds of these two termite species constitute alternative supports alongside the
398 sediments and soils used in geochemical prospecting. The results of this study also show that
399 these termite materials are potential tools for detailed mapping of areas covered.
400 Modelling of the variability of the added-value metals (i.e. Cu and Co) in the region has shown
401 that their enrichment in the termite mounds was due to both species' behaviors: *Macrotermes*
402 tend to go much deeper until they reach zones of sulphide mineralization to obtain materials,
403 whereas *Cubitermes* reached materials in superficial formations, rich in oxidized minerals.
404 Further studies will elucidate the depth to which each of the two species descends to obtain
405 material, with possible implications in a mining prospecting perspective.
406
407

6. Acknowledgments

This study was funded by World Bank PROMINES program entitled: « Regional Study of Three Target Areas in the Democratic Republic of the Congo » (Project number P106982-IDA-H589 ZR). The authors are grateful to the Democratic Republic of Congo's Ministry of Mines for the authorization to valorize these data.

7. References

Armstrong, R.A., Master, S., Robb, L.J., 2005. Geochronology of the Nchanga Granite, and constraints on the maximum age of the Katanga Supergroup, Zambian Copperbelt. Journal of African Earth Sciences, Recent Advances in the Geology and Mineralization of the Central African Copperbelt 42, 32–40.

Arhin, E., Nude, P.M., 2010. Use of termitaria in surficial geochemical surveys: evidence for> 125-µm size fractions as the appropriate media for gold exploration in northern Ghana. Geochemistry: Exploration, Environment, Analysis 10, 401–406.

Arveti, N., Reginald, S., Kumar, K.S., Harinath, V., Sreedhar, Y., 2012. Biogeochemical study of termite mounds: a case study from Tummalapalle area of Andhra Pradesh, India. Environ Monit Assess 184, 2295–2306.

Bachelier, G., 1978. La faune des sols, son écologie et son action. ORSTOM, Initiations-Documents technique N°38, 391.

Batumike, M.J., Cailteux, J.L.H., Kampunzu, A.B., 2007. Lithostratigraphy, basin development, base metal deposits, and regional correlations of the Neoproterozoic Nguba and Kundelungu rock successions, central African Copperbelt. Gondwana Research 11, 432–447.

433 Batumike, M.J., Kampunzu, A.B., Cailteux, J.H., 2006. Petrology and geochemistry of the
434 Neoproterozoic Nguba and Kundelungu Groups, Katangan Supergroup, southeast
435 Congo: Implications for provenance, paleoweathering and geotectonic setting. Journal
436 of African Earth Sciences 44, 97–115.
437 Black, H.I.J., Okwakol, M.J.N., 1997. Agricultural intensification, soil biodiversity and
438 agroecosystem function in the tropics: the role of termites. Applied Soil Ecology, Soil
439 Biodiversity, Agricultural Intensification and Agroecosystem Function 6, 37–53.
440 Bogaert, J., Gilles (éd.), C., Grégory (éd.), M., 2018. Anthropisation des paysages katangais.
441 Presses Agronomiques de Gembloux, 311.
442 Bonewitz, R.L., Rondeau, B., 2013. Roches et minéraux. Larousse, Paris, 352.
443 Bubenicek, L., 1966. Géologie des gisements de fer: Métallogénie ou Géochimie ? Mineral.
444 Deposita 1, 43–55.
445 Callec, Y., Dobmeier, C., Hall, D., Padel, M., Delpomdor, F., Thiéblemont, D., Chevillard, M.,
446 Fournier, E., Colin, S., Ilunga Ngoy, S., Mulindwa Matubila, S., Kyobela Wibyala
447 (CAMI Katanga), J., Mashagiro Kwezi, E. H. (Sec. Général. Mines), Mawaya, P.
448 (CAMI), Badosa, T., (CTCPM) (2018). Carte géologique de la zone cible Katanga Sud
449 à 1/400 000. Ministère des Mines, République Démocratique du Congo.
450 Cailteux, J.L.H., De Putter, T., 2019. The Neoproterozoic Katanga Supergroup (D. R. Congo):
451 State-of-the-art and revisions of the lithostratigraphy, sedimentary basin and
452 geodynamic evolution. Journal of African Earth Sciences 150, 522–531.
453 Cailteux, J.L.H., Kampunzu, A.B., Lerouge, C., Kaputo, A.K., Milesi, J.P., 2005. Genesis of
454 sediment-hosted stratiform copper–cobalt deposits, central African Copperbelt. Journal
455 of African Earth Sciences, Recent Advances in the Geology and Mineralization of the
456 Central African Copperbelt 42, 134–158.

457 Cailteux, J.L.H., Muchez, P., De Cuyper, J., Dewaele, S., De Putter, T., 2018. Origin of the
458 megabreccias in the Katanga Copperbelt (D.R.Congo). Journal of African Earth
459 Sciences 140, 76–93.
460 Dabard, M.-P., 1983. Etude pétrographique et géochimique des roches sédimentaires
461 paléozoïques du massif armoricain presqu'île de Crozon, flanc nord du bassin de Laval
462 (Theses). Université de Rennes 1, 196.
463 Darmendrail, D., Baize, D., Barbier, J., Freyssinet, P., Mouvet, C., Salpéteur, I., Wavrer, P.,
464 2000. Fonds géochimique naturel : État des connaissances à l'échelle nationale (Étude
465 réalisée dans le cadre des actions de Service public du BRGM 99-F-269) (Document
466 public No. BRGM/RP-50158-FR). France.
467 Decree, S., Deloule, E., De Putter, Th., Dewaele, S., Mees, F., Marignac, Ch., 2014. Dating of
468 U-rich heterogenite: New insights into U deposit genesis and U cycling in the Katanga
469 Copperbelt. Precambrian Research Volume 241, February 2014, Pages 17-28
470 Delpomdor, F., Callec, Y., Bailly, L., Mashigiro, E.H., Ilunga, S., Sebagenzi, S., Mupande, J.F.,
471 Kampata, D., Cailteux, J., 2020. Sedimentary evolution and chemostratigraphy of the
472 post-Sturtian cap carbonate-like Dolomie Tigrée Formation (Katanga Supergroup) in
473 the Democratic Republic of the Congo. Journal of African Earth Sciences 162, 103727.
474 De Putter, T., Dewaele, S., Decree, S., Jedwab, J., 2016. Caractérisation géochimique des
475 minerais de cuivre et cobalt de l'Arc Cuprifère katangais (République Démocratique du
476 Congo) et implications génétiques. Réunion des Sciences de la Terre Nancy 2008 3^{e}
477 Colloque de Launay.
478 Demesmaeker, G., Francois, A., Oosterbosch R., 1963. La tectonique des gisements cuprifères
479 stratiformes du Katanga. 1963, 002, 47 A, 115
480 El Desouky, H.A., Muchez, P., Boyce, A.J., Schneider, J., Cailteux, J.L.H., Dewaele, S., von
481 Quadt, A., 2010. Genesis of sediment-hosted stratiform copper–cobalt mineralization at

Luiswishi and Kamoto, Katanga Copperbelt (Democratic Republic of Congo). Miner Deposita 45, 735–763.

Eschenbrenner, V., 1986. Contribution des termites à la microagrégation des sols tropicaux. Cahiers ORSTOM.Série Pédologie 22, 397–408.

Fontaine, L., De Putter, T., Bernard, A., Decrée, S., Cailteux, J., Wouters, J., Yans, J., 2020. Complex mineralogical-geochemical sequences and weathering events in the supergene ore of the Cu–Co Luiswishi deposit (Katanga, D.R. Congo). Journal of African Earth Sciences 161, 103674.

François, A., 1974. Stratigraphie, tectonique et minéralisations dans l'arc cuprifère du Shaba (République du Zaïre), 23.

Garnier-Sillam, E., 1987. Biologie et rôle des termites dans les processus d'humification des sols forestiers tropicaux du Congo (These de doctorat). Paris 12, Paris, 276.

Garnier-Sillam, E., Braudeau, E., Tessier, D., 1991. Rôle des termites sur le spectre poral des sols forestiers tropicaux. Cas de *Thoracotermes macrothorax* Sjöstedt (Termitinae) et de *Macrotermes mülleri* (Sjöstedt) (Macrotermitinae). Ins. Soc 38, 397–412.

Gleeson, C.F., Poulin, R., 1989. Gold exploration in Niger using soils and termitaria. Journal of Geochemical Exploration 31, 253–283.

Granier, C.L., 1962. La terminologie des méthodes de prospections géochimiques. Bulletin de Minéralogie 85, 11–14.

Grassé, P.P., 1950. Termites et Sols tropicaux. Journal d'agriculture traditionnelle et de botanique appliquée 30, 549–554.

Grassé, P.-P., Noirot, C., 1961. Nouvelles recherches sur la systématique et l'éthologie des Termites champignonnistes du genre *Bellicositermes* Emerson. Ins. Soc 8, 311–359.

505 Grunsky, E.C., Smee, B.W., 1999. The differentiation of soil types and mineralization from
506 multi-element geochemistry using multivariate methods and digital topography. Journal
507 of Geochemical Exploration 67, 287–299.
508 Jouquet, P., Bottinelli, N., Lata, J.-C., Mora, P., Caquineau, S., 2007. Role of the fungus-
509 growing termite *Pseudacanthotermes spiniger* (Isoptera, Macrotermitinae) in the
510 dynamic of clay and soil organic matter content. An experimental analysis. Geoderma
511 139, 127–133.
512 Jouquet, P., Lepage, M., Velde, B., 2002. Termite soil preferences and particle selections:
513 strategies related to ecological requirements. Insectes soc. 49, 1–7.
514 Jouquet, P., Tessier, D., Lepage, M., 2004. The soil structural stability of termite nests: role of
515 clays in *Macrotermes bellicosus* (Isoptera, Macrotermitinae) mound soils. European
516 Journal of Soil Biology 40, 23–29.
517 Jouquet, P., Traoré, S., Choosai, C., Hartmann, C., Bignell, D., 2011. Influence of termites on
518 ecosystem functioning. Ecosystem services provided by termites. European Journal of
519 Soil Biology 47, 215–222.
520 Kampunzu, A.B., Cailteux, J., 1999. Tectonic Evolution of the Lufilian Arc (Central Africa
521 Copper Belt) During Neoproterozoic Pan African Orogenesis. Gondwana Research 2,
522 401–421.
523 Kaya Muyumba, D., Liénard, A., Mahy, G., Ngongo Luhembwe, M., Colinet, G., 2015.
524 Caractérisation des systèmes sols-plantes dans les collines de l'arc cuprifère du Katanga
525 (synthèse bibliographique). Biotechnol. Agron. Soc. Environ. 204–214.
526 Key, R.M., Liyungu, A.K., Njamu, F.M., Somwe, V., Banda, J., Mosley, P.N., Armstrong,
527 R.A., 2001. The western arm of the Lufilian Arc in NW Zambia and its potential for
528 copper mineralization. Journal of African Earth Sciences, African Renaissance and
529 Geosciences 33, 503–528.

530 Kipata, M.L., Delvaux, D., Sebagenzi, M.N., Cailteux, J.-J., Sintubin, M., 2016. Late- to post-
531 orogenic extension and inversion in the Lufilian Arc, RDCongo. 24rd Colloquium of
532 African Geology, Addis Ababa, Ethiopia, January 8-14, 2013.
533 Kouassi, A.M., Mamadou, A., Ahoussi, K.E., Biemi, J., 2014. Conception de modèles
534 statistiques a variables hydrochimiques pour la prédiction de la conductivité électrique
535 des eaux souterraines. LARHYSS Journal P-ISSN 1112-3680 / E-ISSN, 2521-9782 0.
536 Larbi, Y., 2003. Caractérisation géochimique (éléments majeurs et éléments en traces), traçage
537 isotopique (Sm-Nd, Lu-Hf) et géochronologie (Pb-Pb, U-Pb) du groupe de Wakeham,
538 N.E. Québec : bassin sédimentaire prétérozoïque dans la province de Grenville (phd).
539 Université du Québec à Chicoutimi., Montréal, 139.
540 Laville-Timsit, 1986. Prospection géochimique statégique des feuilles à 1/50 000 : Mazamet et
541 Saint-Pons (No. GMX/GCA INV285). Mazamet et Saint-Pons, 27.
542 Le Roux, J.P., Hambleton-Jones, B.B., 1991. The analysis of termite hills to locate uranium
543 mineralization in the Karoo Basin of South Africa. Journal of Geochemical
544 Exploration 41, 341–347.
545 Lefebvre, J.J., 1976. Minéralisation cupro-cobaltifère et zincifère d'aspect épigénétique à
546 Kabolela, Shaba, Zaïre, 315–335.
547 Léon, D., 1995. Le gisement de Kinsenda (sud-est du Shaba, Zaïre) : une concentration
548 cuprifère stratoïde dans les formations détritiques du Roan (Protérozoïque supérieur).
549 BRGM Chronique de la recherche minière 521, 19–37.
550 Letalenet, 1986. Prospection stratégique géochimique et alluvionnaire (No. GMX/GCA
551 INV.287). Nouvelle-Calédonie, Koumac, 12.
552 Malaisse, F., 2018. Prologue Le Katanga, une mosaïque d'écosystèmes en mutation : une
553 approche globale : Anthropisation des paysages Katangais. Gembloux, Belgique, 23.

554 Mambwe, P., Milan, L., Batumike, J., Lavoie, S., Jébrak, M., Kipata, L., Chabu, M., Mulongo,
555 S., Lubala, T., Delvaux, D., Muchez, P., 2017. Lithology, petrography and Cu
556 occurrence of the Neoproterozoic glacial Mwale Formation at the Shanika syncline
557 (Tenke Fungurume, Congo Copperbelt; Democratic Republic of Congo). Journal of
558 African Earth Sciences 129, 898–909.
559 Martin, F., Montel, J.-M., De Parseval, P., Seydoux, A.-M., 2020. Minéralogie (2e édition).
560 Moradpouri, F., Mohammad hayati, 2021. A copper porphyry promising zones mapping based
561 on the exploratory data, multivariate geochemical analysis and GIS integration. Applied
562 Geochemistry 132, 105051.
563 Mosser, C., 1980. Étude géochimique de quelques éléments traces dans les argiles des
564 altérations et des sédiments, Sciences Géologiques, bulletins et mémoires. Persée -
565 Portail des revues scientifiques en SHS, 219.
566 Muchez, Ph., Vanderhaeghen, P., El Desouky, H., Schneider, J., Boyce, A., Dewaele, S.,
567 Cailteux, J., 2008. Anhydrite pseudomorphs and the origin of stratiform Cu–Co ores in
568 the Katangan Copperbelt (Democratic Republic of Congo). Miner Deposita 43, 575.
569 Mujinya, B.B., Mees, F., Boeckx, P., Bodé, S., Baert, G., Erens, H., Delefortrie, S., Verdoodt,
570 A., Ngongo, M., Van Ranst, E., 2011. The origin of carbonates in termite mounds of the
571 Lubumbashi area, D.R. Congo. Geoderma 165, 95–105.
572 Mujinya, B.B., Mees, F., Erens, H., Dumon, M., Baert, G., Boeckx, P., Ngongo, M., Van Ranst,
573 E., 2013. Clay composition and properties in termite mounds of the Lubumbashi area,
574 D.R. Congo. Geoderma 192, 304–315.
575 Mwana, A., Vranken, I., Nkulu, J., Luba, F., Kyanika, F., Scott Tshibang Nawej, Flori Mastaki
576 Upite, Jean-Pierre Bulambo Mwema, Jan Bogaert, 2018. L'activité minière au Katanga
577 et la perception de ses impacts à Lubumbashi, Kolwezi, Likasi et Kipushi :
578 Anthropisation des paysages katangais. Gembloux, Belgique, 13.

579 Nalovic, L., Quantin, P., 1972. Evolution géochimique de quelques éléments majeurs et traces
580 dans un sol ferrallitique ferritique de Nouvelle-Calédonie issu de péridotites :
581 interprétation d'observations à l'aide de la microsonde de Castaing. Cahiers
582 ORSTOM.Série Pédologie 10, 389–410.
583 Ngoyi, K., Dejonghe, L., 1995. Géologie et genèse du gisement stratoïde cuprifere de Kinsenda
584 (SE du Shaba, Zaïre), 36.
585 Nicollet, C., 2014. Origine et évolution de la croûte continentale. Bulletin de l'APBG 153–171.
586 Roquin, C., Freyssinet, P., Novikoff, A., Tardy, Y., 1991. Géochimie des termitières et des sols
587 sur cuirasse : application à la prospection géochimique de l'or en Afrique de l'Ouest,
588 Principaux résultats scientifiques et techniques : rapport scientifique 1990/1991.
589 BRGM, Paris, pp. 124–125.
590 Sako, A., Mills, A.J., Roychoudhury, A.N., 2009. Rare earth and trace element geochemistry
591 of termite mounds in central and northeastern Namibia: Mechanisms for micro-nutrient
592 accumulation. Geoderma 153, 217–230.
593 Selley, D., Broughton, D., Scott, R.J., Hitzman, M., Bull, S.W., Large, R.R., McGoldrick, P.J.,
594 Croaker, M., Pollington, N.L., Barra, F., 2005. A new look at the geology of the
595 Zambian Copperbelt. Economic Geology 100, 965–1000.
596 Stewart, A.D., Anand, R.R., 2014. Anomalies in insect nest structures at the Garden Well gold
597 deposit: Investigation of mound-forming termites, subterranean termites and ants.
598 Journal of Geochemical Exploration 140, 77–86.
599 Stewart, A.D., Anand, R.R., Balkau, J., 2012. Source of anomalous gold concentrations in
600 termite nests, Moolart Well, Western Australia: implications for exploration.
601 Geochemistry : Exploration, Environment, Analysis 12, 327–337.

Sikakwe, G.U., Nwachukwu, A.N., Uwa, C.U., Abam Eyong, G., 2020. Geochemical data handling, using multivariate statistical methods for environmental monitoring and pollution studies. Environmental Technology & Innovation 18, 100645.

Tardy, Y., 1997. Petrology of Laterites and Tropical Soils. Balkema, 408 pp.

Taylor, S.R. and McLennan, S.M., 1985. The Continental Crust: Its Composition and Evolution. Blackwell, London, 312 pp.

Thoreau, J., Terdonck, R. du T. de, 1933. Le Gite d'uranium de Shinkolobwe-Kasolo Katanga. Falk, 46.

Twite, F., Broughton, D., Nex, P., Kinnaird, J., Gilchrist, G., Edwards, D., 2019. Lithostratigraphic and structural controls on sulphide mineralisation at the Kamoa copper deposit, Democratic Republic of Congo. Journal of African Earth Sciences 151, 212–224.

Valé, M., 2006. Quantification et prédiction de la minéralisation nette de l'azote du sol in situ, sous divers pédoclimats et systèmes de culture français (thèse). Institut National Polytechnique, Toulouse, 209.

Wendorff, M., 2011. Tectonosedimentary expressions of the evolution of the Fungurume foreland basin in the Lufilian Arc, Neoproterozoic–Lower Palaeozoic, Central Africa. Geological Society, London, Special Publications 357, 69–83.

Figure captions:

Fig. A.1 Height of *Macrotermes* termite mounds

Fig. A.2 Classes of *Macrotermes* termite mounds on the geological map

Fig. A.3 Classes of *Cubitermes* termite mounds on the geological map

Fig. 1 Simplified geological map of the Central African Copperbelt (CACB) and Katangan basin showing locations of major Cu and Co deposits and cities (Wendorff 2011, Twite et al., 2019)

Fig. 2 Simplified geological map of area studied (from 1/200 000 geological sheets : Kayoyo, Ruwe, Sakabinda (Callec et al, 2018b))

Fig. 3 *Macrotermes* termite mounds (a) and *Cubitermes* termite mounds (b) 2017 © Serge Ilunga Ngoy

Fig. 4 Color contrast of *Macrotermes* termite mound series

Fig. 5 Dendrogram of *Macrotermes* termite mound series (a) and *Cubitermes* termite mound series (b)

Fig. 6 Variability of the classes according to the contents of major elements for *Macrotermes* (a) and *Cubitermes* (b) termite mounds

Fig. 7 Identification of geological structures by *Macrotermes* termite mounds on geological background

Fig. 8 Cu distribution in *Macrotermes* termite mounds (a) and Co distribution in *Macrotermes* termite mounds (b)

Fig. 9 Principal component analysis of Cu, Co and eleven variables retained for the two series (Macrotermes termite mounds a and Cubitermes b)

Fig. 10 Variability of Co concentrations versus Sb (a) and Cs (c) and Cu concentrations versus Bi (b) and Th (d) - the *Macrotermes* termite series (a, b) and the *Cubitermes* termite series (c, d)

Tables:

Age (Ma)			Supergroup	Group	Subgroup	Formation	Lithology
542	Lower Palezoic		Biano				sandstones and shales
			Major stratigraphic unconformity				
635	NEOPROTEROZOIC	EDIACARIAN	KATANGA	Kundelungu (Ku)	Ngule (Ku-3)	Sampwe	sandstones and shales Ravinement surface or tectonic unconformity
						Kiubo	sandstones, calcaerous to dolomitic siltstones, dolostones, limestones
						Mongwe	
					Gombela (Ku-2)	Lubudi	dolostones and limestones
						Kaniang a	dolomitic siltstones and shales, dolomitic sandstones
						Lusele	pink dolostone
660		CRYOGENIAN			Kyandamu (Ku-1) "Petit Conglomérat" diamictite (Marinoan glaciation?)		diamictite Ravinement surface
680				Nguba (Ng)	Bunkeya (Ng-3)	Monwezi	calcareous to dolomitic silstones and shales
						Katete	
					Muombe (Ng-2)	Kipushi	dolostones and limestones
						Kakontwe	
						Kapond a	dolomitic siltstones and shales
						Dolomie Tigrée	striped whitish dolostone and shales
730					Mwale (Ng-1) "Grand		diamictite, shales, sandstones, pyritic

				Conglomérat" diamictite (Sturtian glaciation?)		siltstones, basalt Ravinement surface
735		**TONIAN**	**Roan (R)**	**Mwashya (R-4)**	Kanzadi	lenticular sandstones
					Kafubu	carbonaceous shales
					Kamoya	dolomitic siltstones Ravinement surface
765				**Fungurume (R-3)**	Kansuki	dolostones, pyroclastics Ravinement surface or tectonic unconformity
					Mofya	dolostones
					Tenke	dolomitic shales, siltstones, , dolostones, intrusives gabbros
					Dipeta	
					Kwatebala (R.G.S)	clayey siltstones and sandstones
				Mines (R-2)	Kambove (R2.3)	dolostones
					Dolomitic Shales (R-2.2)	dolomitic shales
					Kamoto (R-2.1)	laminated dolostones to dolostones
				Musonoï (R-1)	chloritic dolostones hemaetitic and clayey dolomitic siltstones to sandstones Basal conglomerates of the R.A.T Ravinement surface	
				Basal conglomerates (Nzilo Fm)		

< 883	Major stratigraphic unconformity
Archean or Mesoproterozoic basement (Kibara, Kasaï)	

Table 1 Revised lithostratigraphy of the Katanga Supergroup (Cailteux et De Putter, 2019)

665

	Series	MTM																CTM							
	AHC-Class	I		II		III		IV		V		VI		VII		VIII		I		II		IV		V	
	Effective	9		7		12		5		12		3		7		5		10		9		6		2	
	D.L.	Mean	Std. Dev.	Mean	Std. Dev.	Mean	Std. Dev.	Mean	Std. Dev.	Mean	Std. Dev.	Mean	Std. Dev.	Mean	Std. Dev.	Mean	Std. Dev.	Mean	Std. Dev.	Mean	Std. Dev.	Mean	Std. Dev.	Mean	Std. Dev.
Ag (ppm)	**0,01-100**	0,037	0,02	0,04	0,02	0,04	0,02	0,084	0,04	0,04	0,01	0,07	0,01	0,041	0,02	0,04	0,01	0,047	0,01	0,043	0,01	0,048	0,02	0,05	0,01
Al (%)	**0,01-50**	6,902	1	8,19	0,57	8,102	1,1	7,902	1,08	10,8	0,55	7,93	0,33	11,14	0,88	9,62	1,1	7,694	0,98	6,842	1,44	6,923	1,04	8,69	0,6
As (ppm)	**0,2-10000**	4,8	1,82	4,671	2,82	3,808	1,4	10,62	2,85	5,38	1,74	4,87	0,5	2,971	1,68	2,18	0,42	3,18	1,18	2,889	1,19	1,617	0,39	1,1	0,14
Ba (ppm)	**10-10000**	48,89	42,26	60	20,82	230,8	67,35	84	30,5	163	65,27	340	10	181,4	64,66	96	23,02	101	35,42	103,3	48,99	231,7	64,01	155	7,07
Be (ppm)	**0,05-1000**	0,588	0,17	0,397	0,09	1,074	0,34	0,75	0,3	0,8	0,2	1,28	0,03	0,84	0,2	0,59	0,12	0,71	0,26	0,616	0,22	1,192	0,2	1,06	0,35
Bi (ppm)	**0,01-10000**	0,18	0,07	0,331	0,04	0,358	0,04	0,608	0,28	0,4	0,11	0,32	0,03	0,609	0,14	0,39	0,1	0,351	0,03	0,262	0,05	0,312	0,03	0,38	0,02
Ca (%)	**0,01-50**	0,042	0,02	0,077	0,08	0,12	0,08	0,054	0,03	0,07	0,04	0,1	0,02	0,124	0,06	0,06	0,06	0,029	0,01	0,031	0,02	0,033	0,02	0,03	0,01
Cd (ppm)	**0,02-1000**	0,016	0,01	0,026	0,02	0,02	0,01	0,026	0,01	0,02	0,01	0,02	0,02	0,016	0,01	0,03	0,02	0,037	0,03	0,046	0,02	0,052	0,02	0,1	0,04
Ce (ppm)	**0,01-500**	116,1	70,56	48,61	15,23	77,71	20,26	68,8	15,82	57,1	34,67	98,3	2,92	73,76	13,45	46,4	11,44	44,3	7,29	47,48	16,9	61,22	8,74	62,2	26,59
Co (ppm)	**0,1-10000**	7,2	2,53	2,686	0,63	3,842	0,97	6,78	2,76	5,33	1,62	7,27	1,1	9,7	4,17	7,34	2,49	3,72	1,32	3,067	0,82	4,117	0,95	7,9	2,4
Cr (ppm)	**1-10000**	41,22	15,48	46,43	5,56	57,17	9,08	61,6	11,46	64,3	7,57	54	2,65	54,86	5,37	45,4	4,39	50,4	5,27	47,33	7,25	54,5	5,75	65	4,24
Cs (ppm)	**0,05-500**	1,187	0,51	1,996	0,36	4,95	2,15	2,394	0,58	5,88	1,21	2,37	0,28	7,743	2,37	6,39	0,96	4,475	0,68	3,444	0,84	5,008	1,34	7,21	0,52
Cu (ppm)	**0,2-10000**	29,16	11,38	26,59	6,13	37,86	17,94	59,52	29,04	48,6	17,21	46,4	4,62	162,9	122,47	108	37,61	26,15	5,73	27,74	8,14	39,73	7,83	71,3	3,82
Fe (%)	**0,01-50**	3,279	1,27	1,574	0,55	2,845	1,22	4,336	0,89	3,79	2,07	7,84	0,81	2,404	0,88	1,59	0,41	1,618	0,47	1,911	0,85	1,712	0,34	1,14	0,14
Ga (ppm)	**0,05-10000**	20,61	4,12	19,3	1,01	20,82	2,79	21,14	2,36	26,7	2,95	21,7	1,14	29,16	2,65	20,8	1,67	17,97	1,67	15,26	2,03	17,58	3,02	21,9	1,34
Ge (ppm)	**0,05-500**	0,104	0,02	0,074	0,02	0,115	0,02	0,078	0,01	0,09	0,02	0,14	0	0,121	0,03	0,09	0,02	0,074	0,01	0,077	0,01	0,112	0,01	0,12	0,02
Hf (ppm)	**0,1-500**	3,811	0,73	5,229	0,48	5,867	0,68	4,94	0,3	6,74	0,62	6	0,1	7,986	0,55	6,56	0,64	5,15	0,39	4,633	0,69	4,733	0,28	4,95	0,21
In (ppm)	**0,005-500**	0,034	0,01	0,077	0	0,095	0,02	0,106	0,04	0,11	0,02	0,11	0,01	0,114	0,02	0,08	0,02	0,067	0,01	0,051	0	0,054	0,01	0,07	0
K (%)	**0,01-10**	0,278	0,29	0,241	0,1	1,252	0,41	0,67	0,3	0,87	0,23	1,13	0,03	0,67	0,25	0,47	0,27	0,644	0,29	0,623	0,33	1,285	0,32	0,64	0,04
La (ppm)	**0,5-10000**	44,24	21,55	22,6	8,68	33,48	8,57	19,18	1,7	17,4	9,52	46,4	0,89	33,81	9,95	23,1	12,19	19,4	6,8	19,61	6,4	28,48	6,9	28,5	12,16
Li (ppm)	**0,2-10000**	13,22	13,17	6,714	1,12	29,53	10,71	14,64	4,86	24,1	11,26	34,8	4,1	78,76	24,97	50,2	24,89	12,53	6,12	9,844	3,56	13,22	1,45	20,2	3,32
Mg (%)	**0,01-50**	0,21	0,21	0,103	0,03	0,321	0,08	0,204	0,08	0,24	0,05	0,27	0,01	0,247	0,05	0,17	0,05	0,173	0,07	0,176	0,05	0,272	0,05	0,17	0,01
Mn (ppm)	**5-100000**	164,3	94,18	122,7	29,2	206,2	95,58	181,8	77,32	153	49,18	444	102,5	193,1	84,33	203	156,93	96,8	44,23	95,44	43,93	106,7	33,46	70	19,8
Mo (ppm)	**0,05-10000**	1,468	0,52	1,35	0,39	1,159	0,3	2,582	0,94	1,93	0,74	2,3	0,4	1,219	0,41	1,02	0,26	1,065	0,28	0,788	0,19	0,515	0,12	0,75	0,27
Na (%)	**0,01-10**	0,014	0,01	0,013	0,01	0,023	0,01	0,016	0,01	0,02	0	0,02	0	0,017	0	0,01	0	0,014	0,01	0,014	0,01	0,023	0,01	0,01	0

Nb (ppm)	**0,1-500**	12,88	3,5	20,7	3,89	21,14	5,62	15,42	4,82	29,8	5,78	37,9	2,85	41,07	4,97	39,7	8,38	20,68	3,19	21,01	10,78	17,83	3,95	28,1	0,71
Ni (ppm)	**0,2-10000**	72,53	49,16	17,86	3,13	21,66	7,44	21,44	4,14	34,8	8,31	27,8	1,66	62,13	9,43	52	26,27	21,55	5,73	17,97	4,61	22,5	3,78	37,7	1,91
P (ppm)	**10-10000**	275,6	62,47	211,4	41,8	246,7	86,69	274	48,27	287	82,5	700	36,06	272,9	74,55	250	18,71	283	63,6	270	56,12	355	59,25	470	42,43
Pb (ppm)	**0,5-10000**	6,1	1,91	12,51	2,98	7,783	1,44	12,32	2,75	9,89	1,34	9	0,52	9,943	1,28	10,1	1,33	9,57	1,77	8,744	1,71	8,767	0,89	13,2	0,49
Rb (ppm)	**0,1-10000**	16,6	17,19	20,36	7,77	98,48	16,77	52,06	15,56	86,2	20,11	81,7	4,73	76,57	28,85	52,7	24,86	67,17	26,93	58,14	25,34	101,6	20,66	83,9	3,89
S (%)	**0,01-10**	0,016	0,01	0,02	0,02	0,014	0,01	0,016	0,01	0,02	0,01	0,02	0	0,019	0,01	0,02	0,01	0,016	0,01	0,018	0	0,018	0	0,03	0
Sb (ppm)	**0,05-10000**	0,463	0,07	0,769	0,12	1,017	0,55	1,014	0,25	1,13	0,32	0,61	0,07	0,623	0,05	0,58	0,07	1,075	0,13	0,812	0,19	0,722	0,03	0,77	0,01
Sc (ppm)	**0,1-10000**	12,69	1,96	15,46	2,38	18,7	2,72	18,92	1,54	22,3	3,32	20,3	0,57	25,06	2,6	18,1	1,54	14,33	1,3	12,64	1,25	15,27	2,19	16,7	0,49
Sn (ppm)	**0,2-500**	2,011	0,36	3,029	0,3	4,017	1,2	2,78	0,5	4,83	0,63	3,23	0,12	5,343	0,48	4,12	0,46	4,08	0,48	2,944	0,57	3,083	0,45	4,15	0,21
Sr (ppm)	**0,2-10000**	19,47	7,82	16,37	7,69	23,27	6,21	17,58	11,73	15,9	3,38	29,1	4,25	22,16	3,77	11,9	4,86	11,28	2,39	11,5	3,75	21	5,87	12,4	0,71
Ta (ppm)	**0,05-100**	0,887	0,21	1,427	0,23	1,427	0,28	1,058	0,33	1,99	0,33	2,5	0,21	2,649	0,33	2,45	0,4	1,446	0,18	1,359	0,52	1,198	0,25	1,85	0,07
Th (ppm)	**0,2-10000**	10,72	1,38	13,39	1,14	12,78	1,29	13,4	1,72	14	2,66	13,1	0,16	16,84	1,58	14,3	1,5	13,61	1	11,85	0,66	13,97	1,37	16,6	0,21
Ti (%)	**0,005-10**	0,348	0,08	0,6	0,09	0,59	0,1	0,436	0,1	0,81	0,14	1,18	0,09	0,975	0,14	0,94	0,11	0,62	0,08	0,6	0,19	0,502	0,07	0,73	0,04
Tl (ppm)	**0,02-10000**	0,128	0,06	0,194	0,06	0,557	0,16	0,256	0,03	0,57	0,12	0,38	0,05	0,497	0,09	0,32	0,04	0,417	0,11	0,343	0,11	0,557	0,1	0,51	0,02
U (ppm)	**0,1-10000**	2,456	0,75	3,114	0,87	3,6	0,72	3,62	0,65	3,7	0,56	3,67	0,31	4,3	0,79	3,48	0,47	3,59	0,82	3,289	0,77	4,617	1,57	3,45	0,35
V (ppm)	**1-10000**	71,78	15,11	69,71	15,89	111,6	20,08	146	25,73	145	33,36	165	6,66	104,7	25,06	74,2	19,97	83,7	17,83	81,22	20,95	73,83	8,08	61,5	6,36
W (ppm)	**0,1-10000**	1,056	0,19	1,886	0,25	2,117	0,55	1,42	0,28	2,55	0,37	1,87	0,06	2,971	0,26	2,38	0,23	2,48	0,3	1,789	0,41	1,733	0,29	2,5	0,14
Y (ppm)	**0,1-500**	13,63	1,98	13,97	2,42	23,92	3,98	15,32	2,52	18	4,9	23,4	1,01	28,63	5,63	22,3	5,91	16,82	3,15	15,28	2,21	23,68	4,38	22,1	6,29
Zn (ppm)	**2-10000**	14,33	4,21	21,14	3,24	23,25	5,66	20,2	4,97	27,8	3,72	34	2,65	41,43	11,36	31,6	4,83	23,3	2,95	19,78	3,87	24,5	1,05	34,5	3,54
Zr (ppm)	**0,5-500**	137,1	25,61	177,4	15,02	200,2	23,18	175,4	7,28	234	24,34	225	4,04	272,3	15,98	233	21,15	178,8	11,99	164,5	27,5	170,5	8,49	177	6,36

Table 2 Summary statistics of two sampling series: MTM: *Macrotermes* Termite Mounds, CTM: *Cubitermes* Termite Mounds, D.L.: detection limit, Std. Dev.: standard deviation

672

	T&McL (Taylor and McLennan, 1985)	Series	MTM								CTM			
		AHC-Class	I	II	III	IV	V	VI	VII	VIII	I	II	IV	V
TiO_2 (%)	0,50		0,57	0,98	0,97	0,72	1,33	1,94	1,60	1,54	1,02	0,98	0,82	1,20
Al_2O_3 (%)	15,20		26,23	31,12	30,79	30,03	41,04	30,15	42,33	36,56	29,24	26,00	26,31	33,02
FeO (%)	4,50		4,23	2,03	3,67	5,59	4,89	10,12	3,10	2,05	2,09	2,47	2,21	1,47
MgO (%)	2,20		0,35	0,17	0,53	0,34	0,40	0,44	0,41	0,28	0,29	0,29	0,45	0,28
CaO (%)	4,20		0,06	0,11	0,17	0,08	0,10	0,14	0,17	0,08	0,04	0,04	0,05	0,04
Na_2O (%)	3,90		0,04	0,04	0,06	0,04	0,05	0,05	0,05	0,03	0,04	0,04	0,06	0,03
K_2O (%)	3,40		0,67	0,58	3,00	1,61	2,09	2,71	1,61	1,13	1,55	1,50	3,08	1,54
			32,14	35,03	39,19	38,4	49,9	45,55	49,27	41,67	34,25	31,32	32,98	37,58
SiO_2 (%)	66,00													
Pseudo-SiO_2 (%)		Reste	67,86	64,97	60,81	61,6	50,1	54,45	50,73	58,33	65,75	68,68	67,02	62,42

673 **Table 3** Comparison of the average major element contents of the different classes defined by
674 AHC in the two types of termite mounds with the average of the upper continental crust (Taylor
675 et McLennan, 1985). In the lower line, the difference between the sum of oxides and 100%
676 gives an approximate value for the SiO_2 content,given that the considered elements represent
677 more than 99% of the total mass of the continental crust

678

	T&McL (Taylor and McLennan, 1985)	Series	MTM								CTM			
		AHC-Class	I	II	III	IV	V	VI	VII	VIII	I	II	IV	V
As (ppm)	1,5		4,80	4,67	3,81	10,62	5,38	4,87	2,97	2,18	3,18	2,89	1,62	1,10
Bi (ppm)	0,127		0,18	0,33	0,36	0,61	0,40	0,32	0,61	0,39	0,35	0,26	0,31	0,38
Cs (ppm)	3,7		1,19	2,00	4,95	2,39	5,88	2,37	7,74	6,39	4,48	3,44	5,01	7,21
Hf (ppm)	5,8		3,81	5,23	5,87	4,94	6,74	6,00	7,99	6,56	5,15	4,63	4,73	4,95
Sb (ppm)	0,2		0,46	0,77	1,02	1,01	1,13	0,61	0,62	0,58	1,08	0,81	0,72	0,77
Th (ppm)	10,7		10,72	13,39	12,78	13,40	14,00	13,08	16,84	14,30	13,61	11,85	13,97	16,60
U (ppm)	2,8		2,46	3,11	3,60	3,62	3,70	3,67	4,30	3,48	3,59	3,29	4,62	3,45
Zr (ppm)	190		137,10	177,40	200,20	175,40	234,00	224,70	272,30	233,00	178,80	164,50	170,50	177,00

679 **Table 4** Seven trace elements are retained for the different classes of two series of termite
680 mounds whose concentrations are higher than the average for the upper continental crust
681 (Taylor and McLennan, 1985)

682

683

		Source	Value	Standard error (%)	Lower bound (95%)	Upper bound (95%)
MTM	Co	Intercept	8,200	0,870	6,459	9,941
		Sb	-2,794	0,961	-4,718	-0,870
	Cu	Intercept	-24,642	15,569	-55,807	6,522
		Bi	218,484	36,822	144,776	292,191
CTM	Co	Intercept	-0,096	0,802	-1,746	1,555
		Cs	0,897	0,173	0,541	1,253
	Cu	Intercept	-41,961	18,118	-79,275	-4,647

Th	5,632	1,351	2,849	8,414

Table 5 Parameters for four linear regression models: MTM: *Macrotermes* Termite Mounds, CTM: *Cubitermes* Termite Mounds

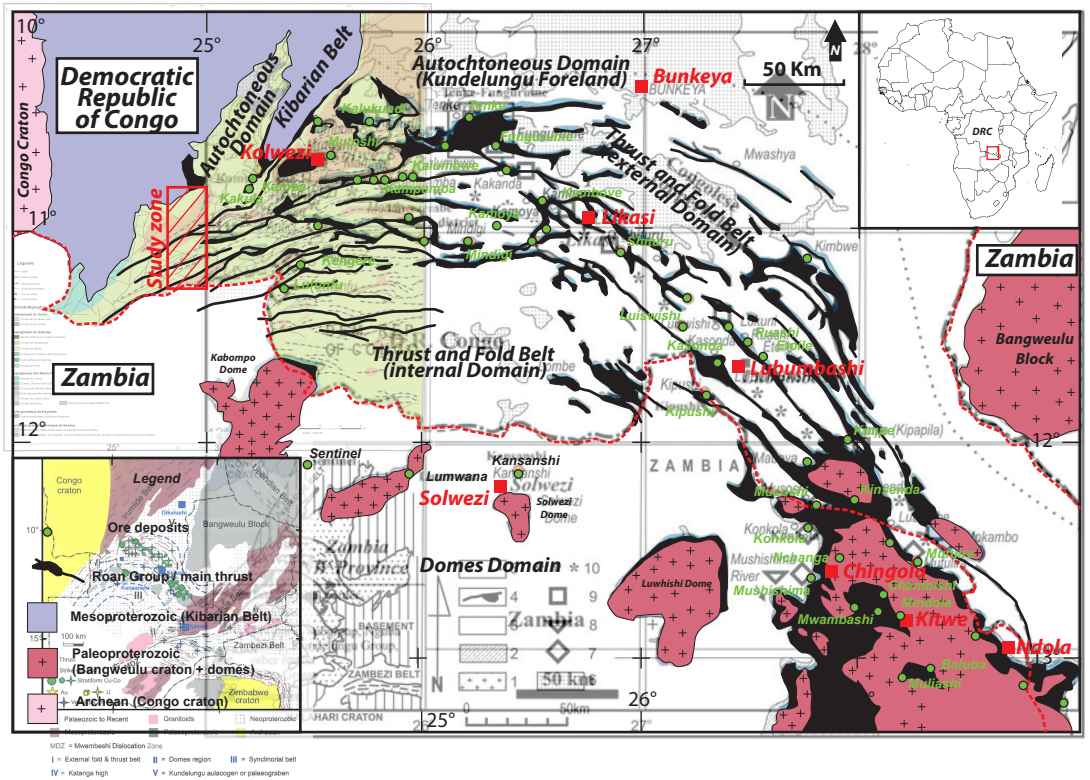
Democratic Republic of Congo
Congo Craton
Autochtoneous Domain
Kibarian Belt
Kolwezi
Kakula
Kengere
Study zone
Zambia
Kabompo Dome
Autochtoneous Domain (Kundelungu Foreland)
Bunkeya
50 Km
Thrust and Fold Belt (External Domain)
Likasi
Thrust and Fold Belt (internal Domain)
Lubumbashi
Kipushi
Kimbwe
Zambia
Bangweulu Block
Kitwe
Ndola
Chingola
Mwambashi
Nchanga
Konkola
Luwhishi Dome
Kansanshi
Lumwana
Solwezi
Solwezi Dome
Sentinel
Domes Domain
ZAMBIA
DRC
Legend
Ore deposits
Roan Group / main thrust
Mesoproterozoic (Kibarian Belt)
Paleoproterozoic (Bangweulu craton + domes)
Archean (Congo craton)
Zambezi Belt
Zimbabwe craton
Congo craton
Bangweulu Block
ZAMBEZI BELT
BASEMENT
50 km
50km

LOCAL GEOLOGY

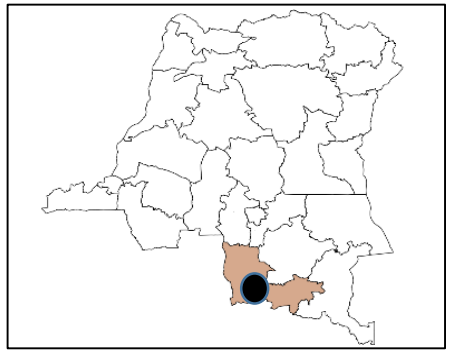

- Sampling points
- Sd — Surfical deposits (as Kalahari sands)
- Ku-1 — Kundelungu Group – Kyandamu Subgroup
- Ku/U — Undifferentiated Kundelungu Group
- Ng-3 — Nguba Group – Bunkeya Subgroup
- Ng-2/U — Nguba Group - Undifferentiated Muombe Subgroup
- Ng-1 — Nguba Group - Mwale Subgroup
- Ng/U — Undifferentiated Nguba Group
- R/U — Undifferentiated Roan Group
- Md — Mezoproterozoic dolerite intrusion
- Ki — Geophysical domain fairly homogeneous fairly magnetic (Kibarian terrains)

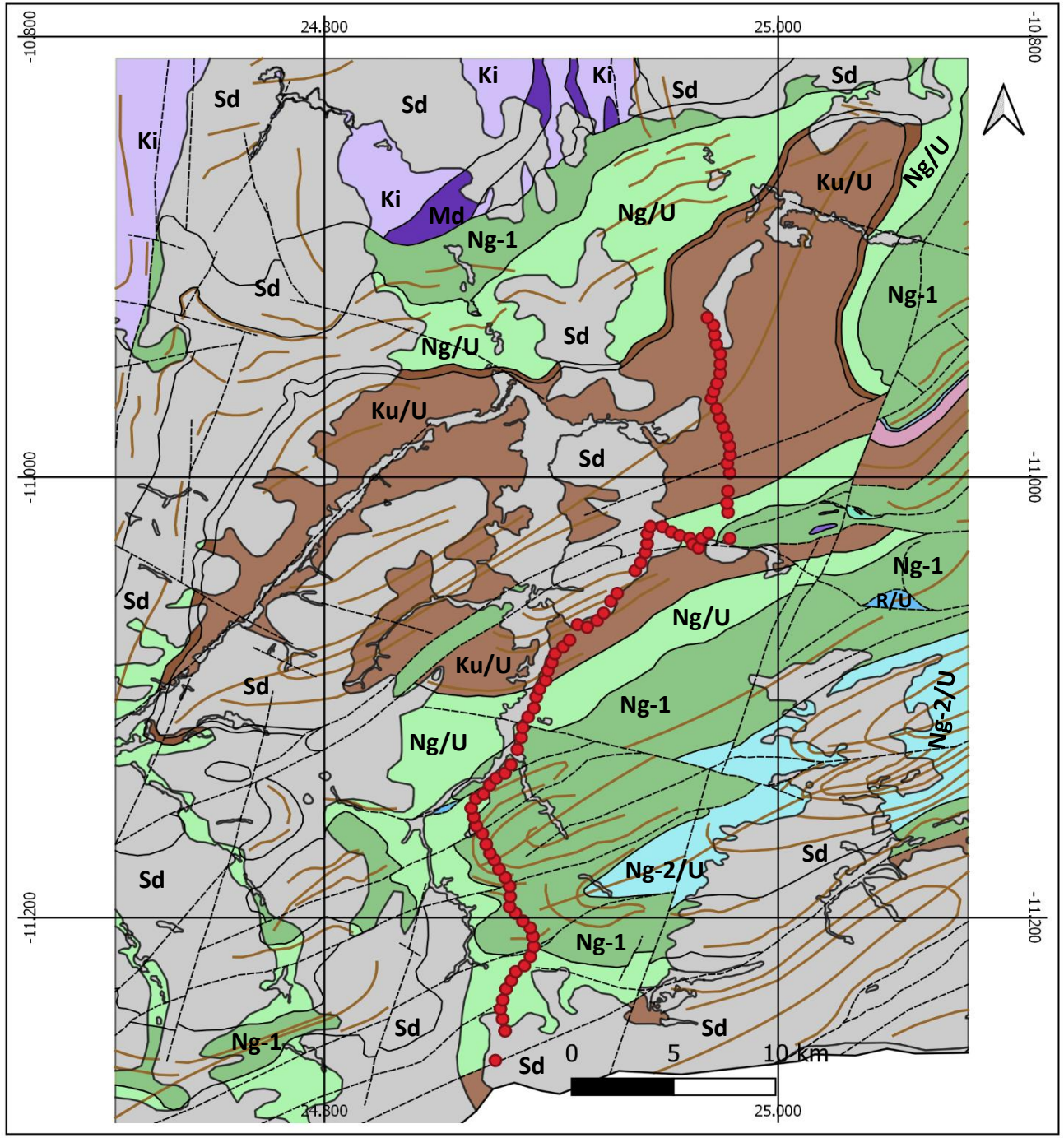

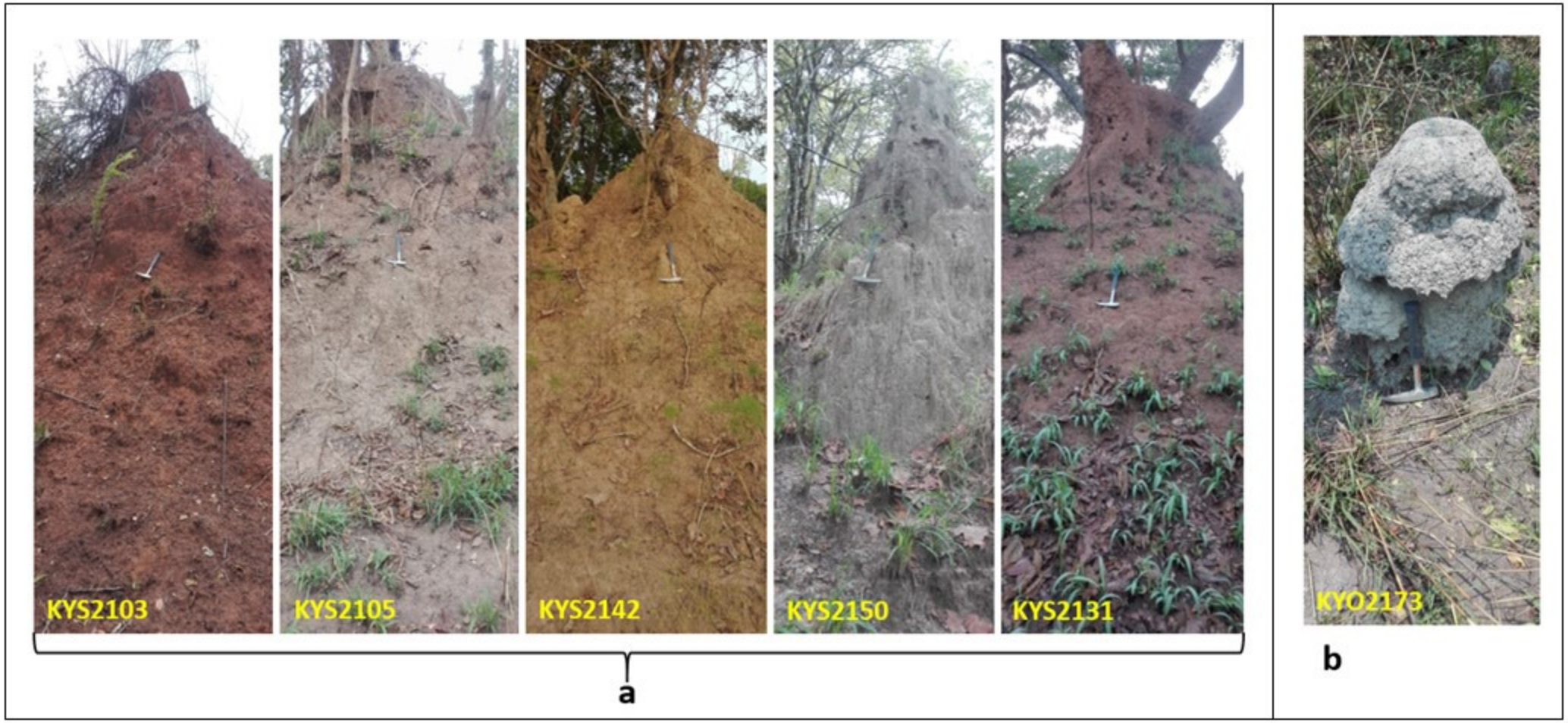
KYS2103
KYS2105
KYS2142
KYS2150
KYS2131
a
KYO2173
b

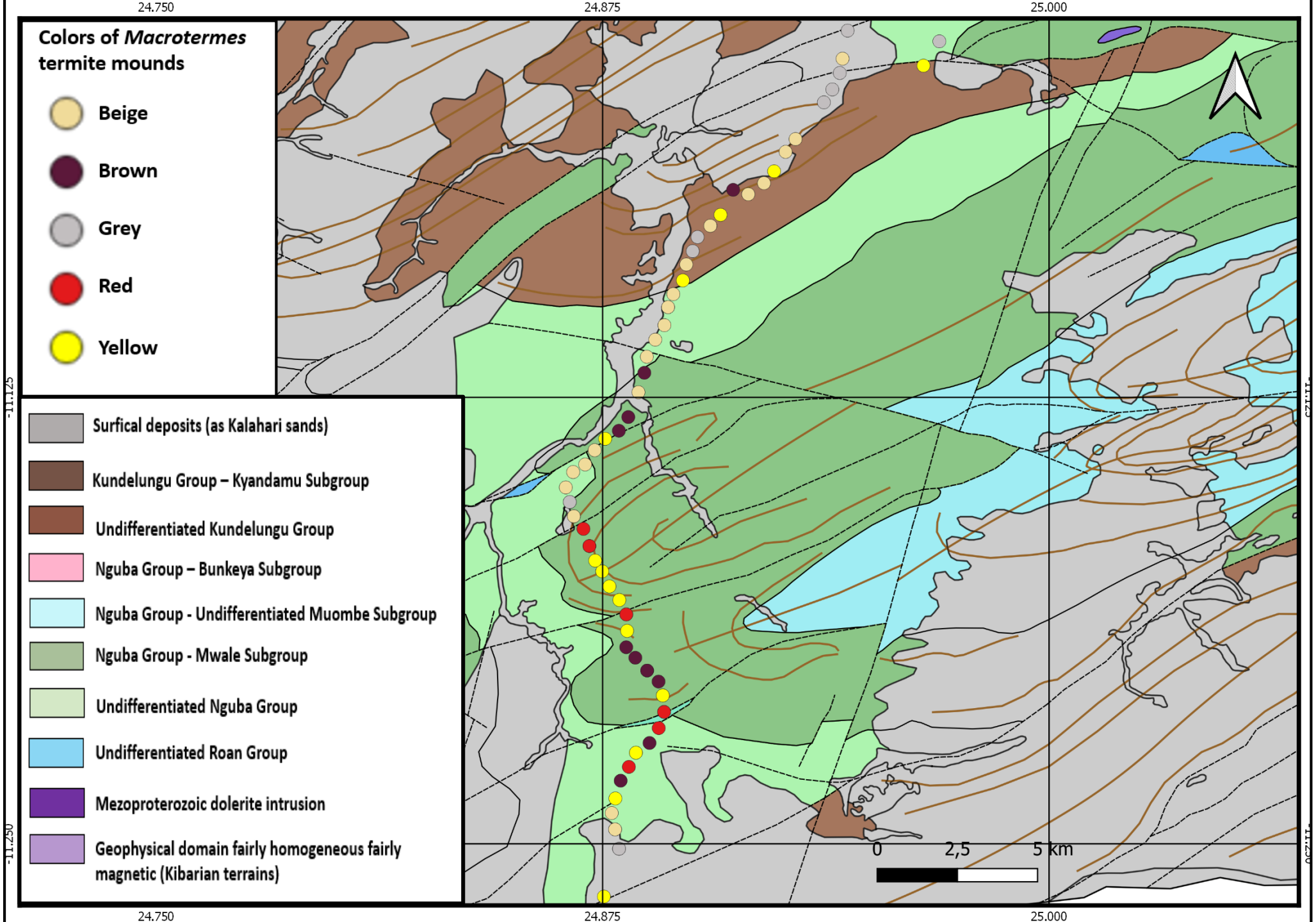
24.750
24.875
25.000
-11.125
-11.250
Colors of *Macrotermes* termite mounds
Beige
Brown
Grey
Red
Yellow
Surfical deposits (as Kalahari sands)
Kundelungu Group – Kyandamu Subgroup
Undifferentiated Kundelungu Group
Nguba Group – Bunkeya Subgroup
Nguba Group - Undifferentiated Muombe Subgroup
Nguba Group - Mwale Subgroup
Undifferentiated Nguba Group
Undifferentiated Roan Group
Mezoproterozoic dolerite intrusion
Geophysical domain fairly homogeneous fairly magnetic (Kibarian terrains)
0
2,5
5 km

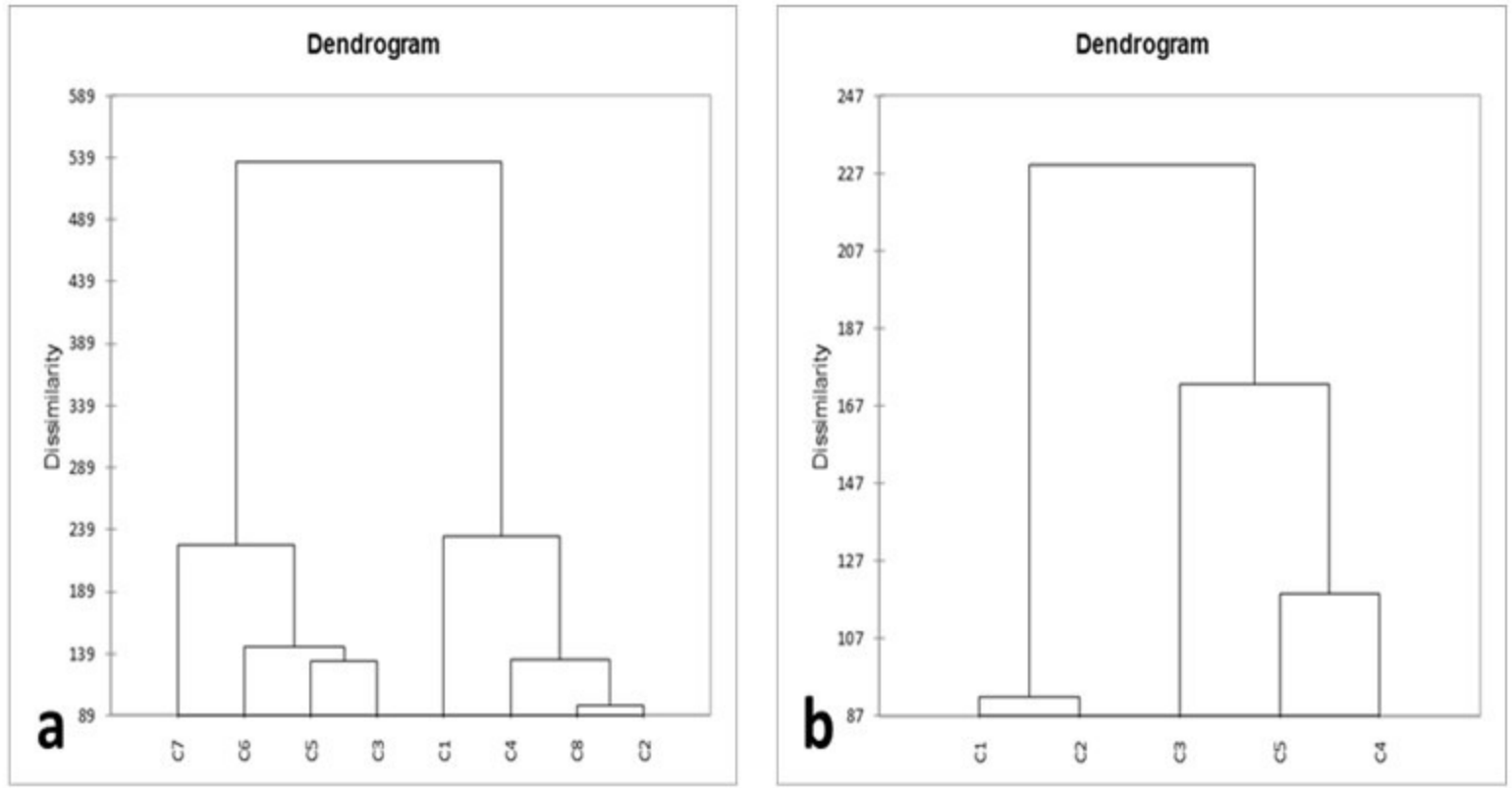
Dendrogram
Dissimilarity
589
539
489
439
389
339
289
239
189
139
89
C7
C6
C5
C3
C1
C4
C8
C2
a
Dendrogram
Dissimilarity
247
227
207
187
167
147
127
107
87
C1
C2
C3
C5
C4
b

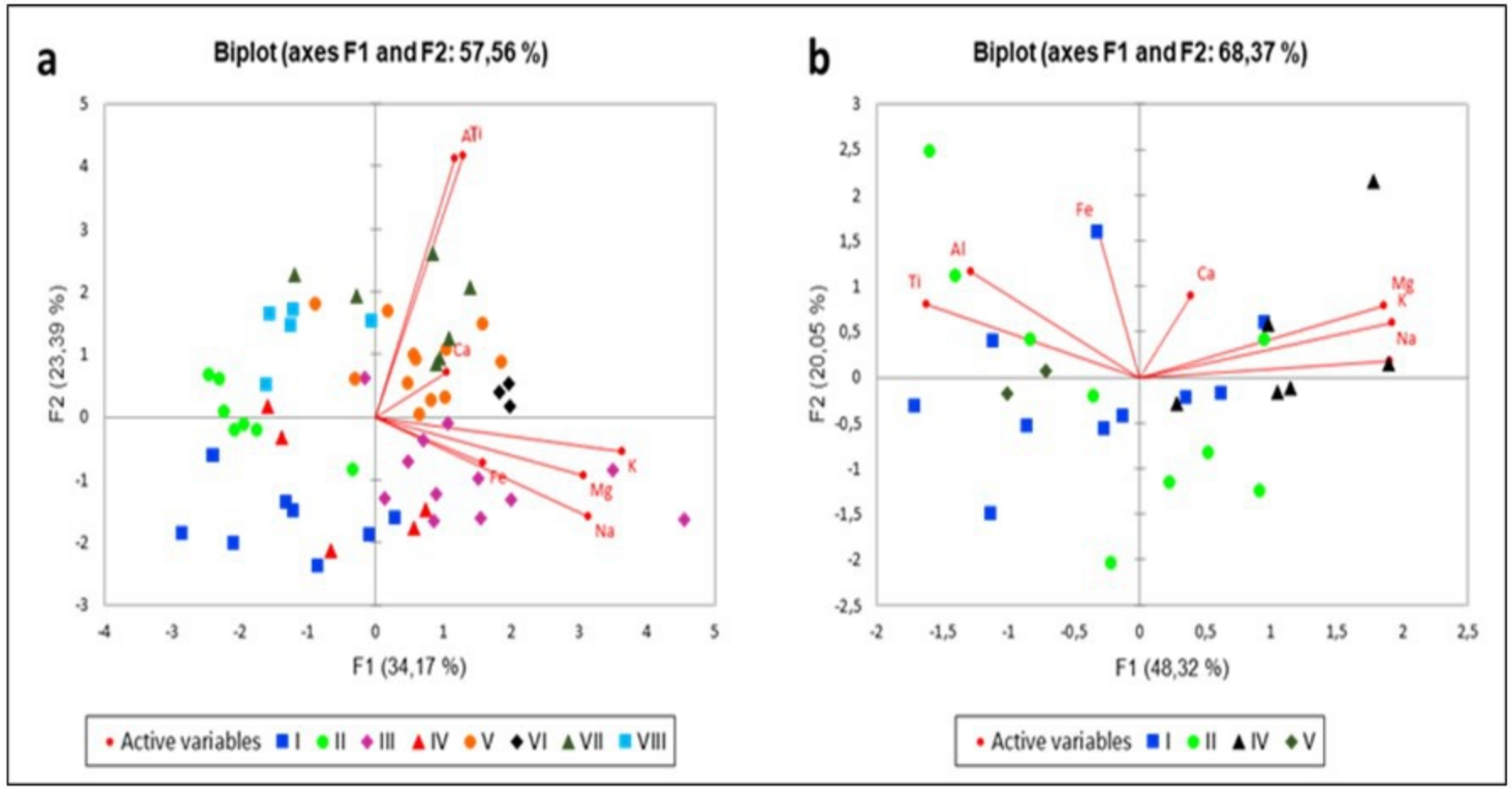
a
Biplot (axes F1 and F2: 57,56 %)
F2 (23,39 %)
F1 (34,17 %)
Al
Ca
Fe
K
Mg
Na
Active variables
I
II
III
IV
V
VI
VII
VIII
b
Biplot (axes F1 and F2: 68,37 %)
F2 (20,05 %)
F1 (48,32 %)
Al
Ca
Fe
K
Mg
Na
Ti
Active variables
I
II
IV
V

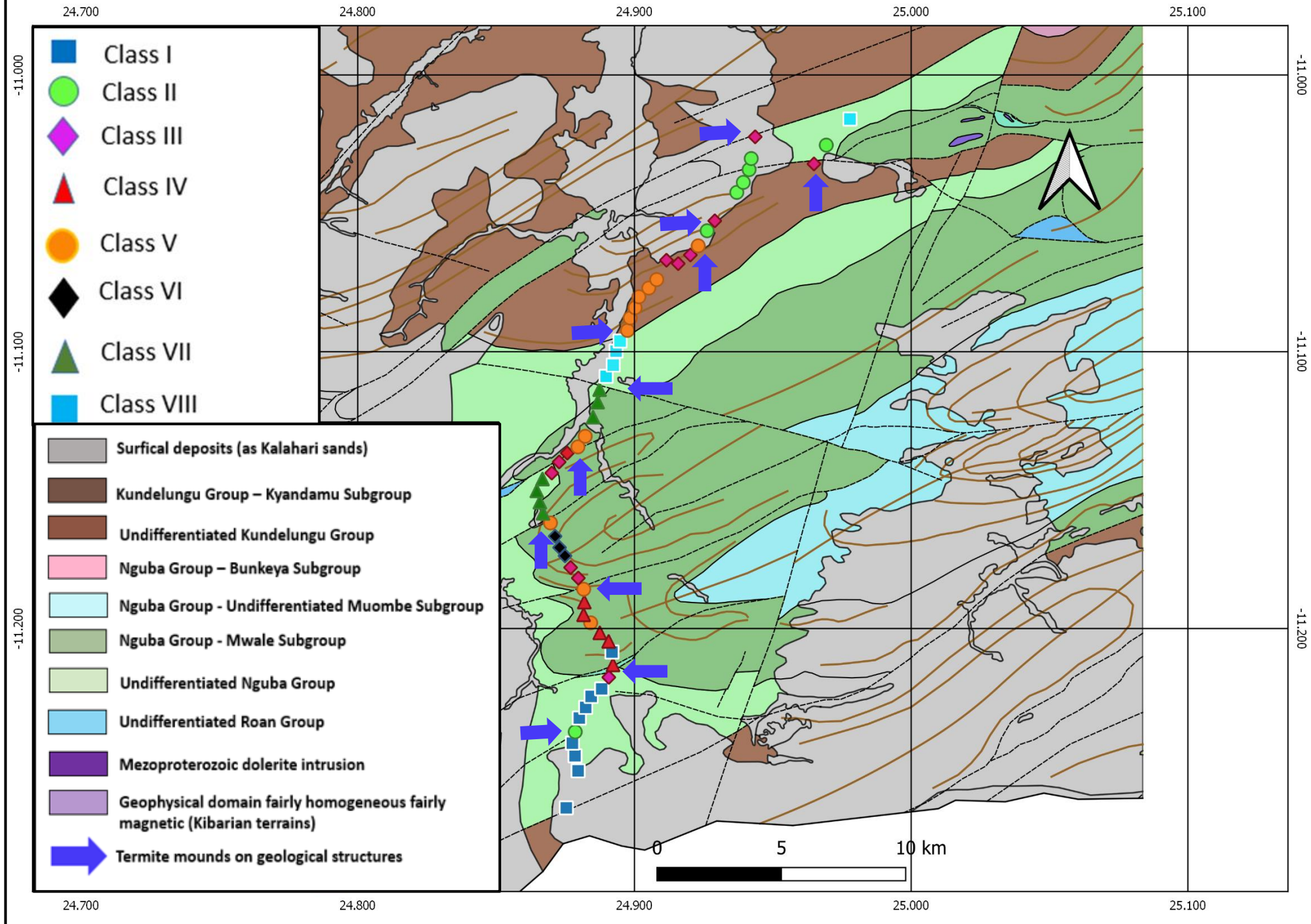
24.700
24.800
24.900
25.000
25.100
-11.000
-11.100
-11.200
Class I
Class II
Class III
Class IV
Class V
Class VI
Class VII
Class VIII
Surfical deposits (as Kalahari sands)
Kundelungu Group – Kyandamu Subgroup
Undifferentiated Kundelungu Group
Nguba Group – Bunkeya Subgroup
Nguba Group - Undifferentiated Muombe Subgroup
Nguba Group - Mwale Subgroup
Undifferentiated Nguba Group
Undifferentiated Roan Group
Mezoproterozoic dolerite intrusion
Geophysical domain fairly homogeneous fairly magnetic (Kibarian terrains)
Termite mounds on geological structures
0
5
10 km

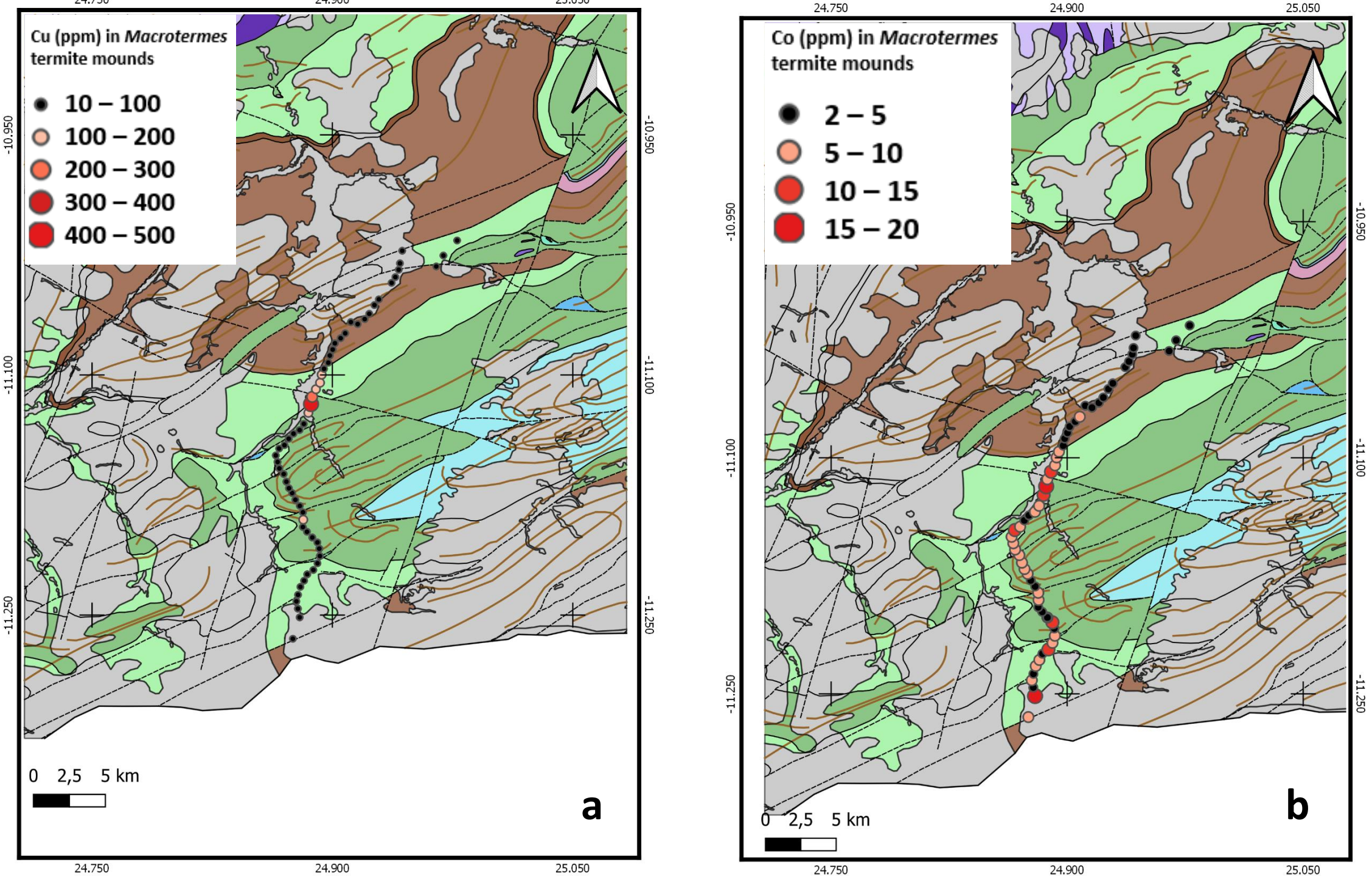
Cu (ppm) in *Macrotermes* termite mounds
10 – 100
100 – 200
200 – 300
300 – 400
400 – 500
0 2,5 5 km
a
Co (ppm) in *Macrotermes* termite mounds
2 – 5
5 – 10
10 – 15
15 – 20
0 2,5 5 km
b
24.750
24.900
25.050
-10.950
-11.100
-11.250

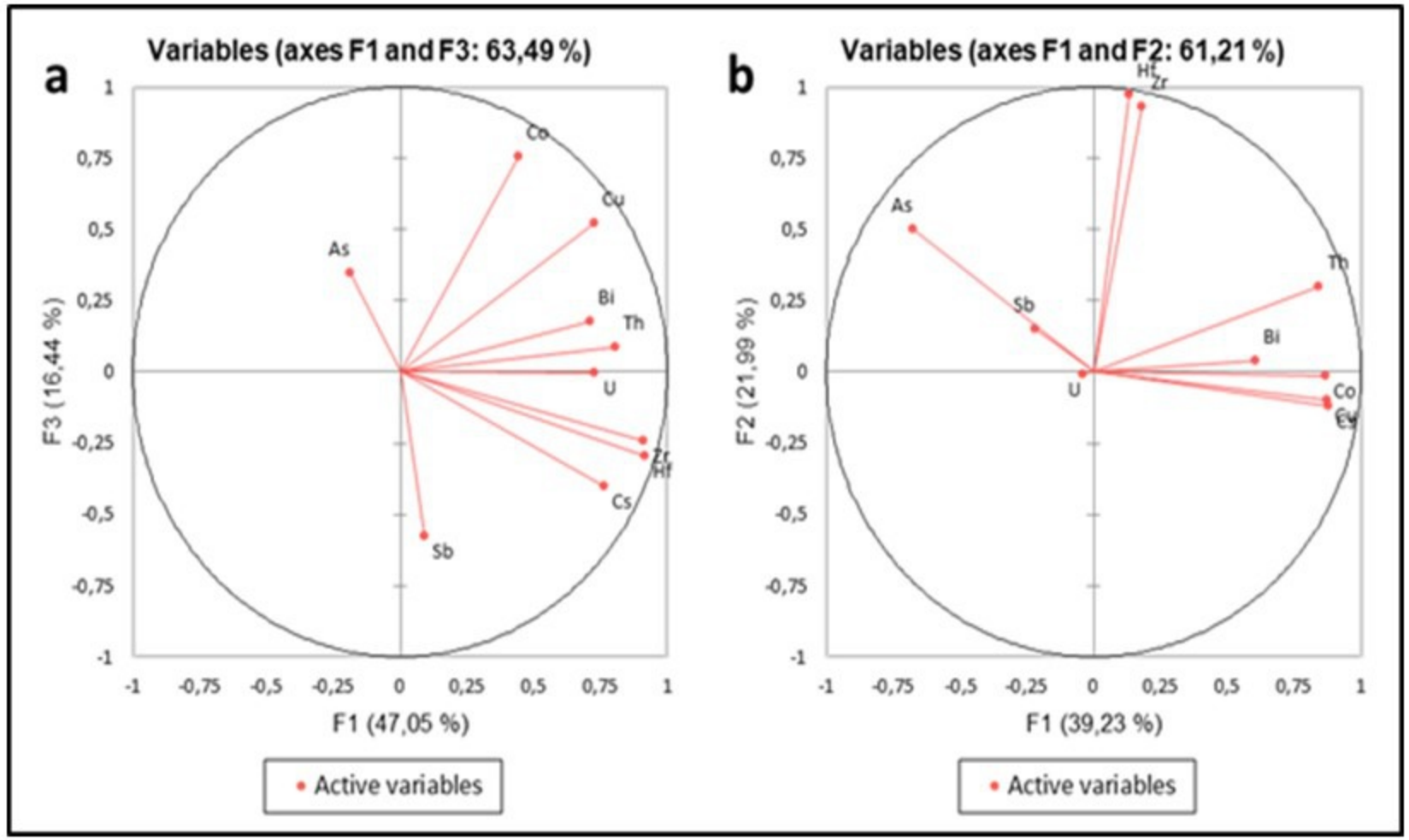
a
Variables (axes F1 and F3: 63,49 %)
F3 (16,44 %)
F1 (47,05 %)
Co
Cu
As
Bi
Th
U
Zr
Hf
Cs
Sb
Active variables
b
Variables (axes F1 and F2: 61,21 %)
F2 (21,99 %)
F1 (39,23 %)
Hf
Zr
As
Th
Sb
Bi
U
Co
Cu
Cs
Active variables

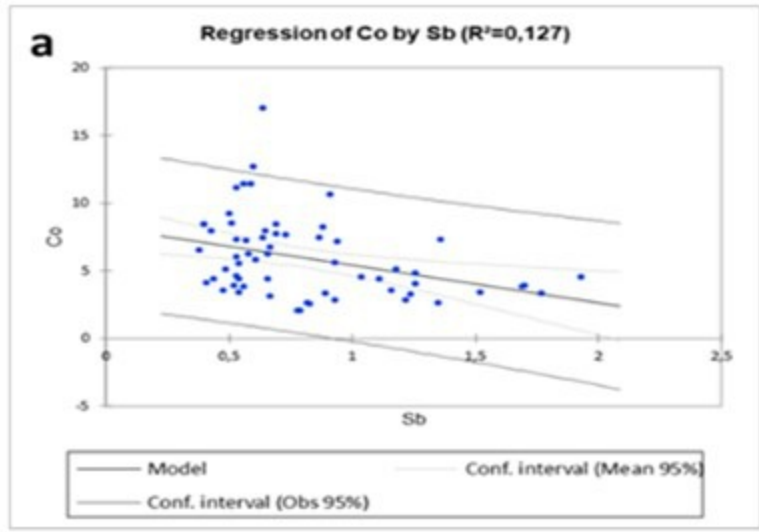
a
Regression of Co by Sb (R²=0,127)
Co
Sb
Model
Conf. interval (Mean 95%)
Conf. interval (Obs 95%)

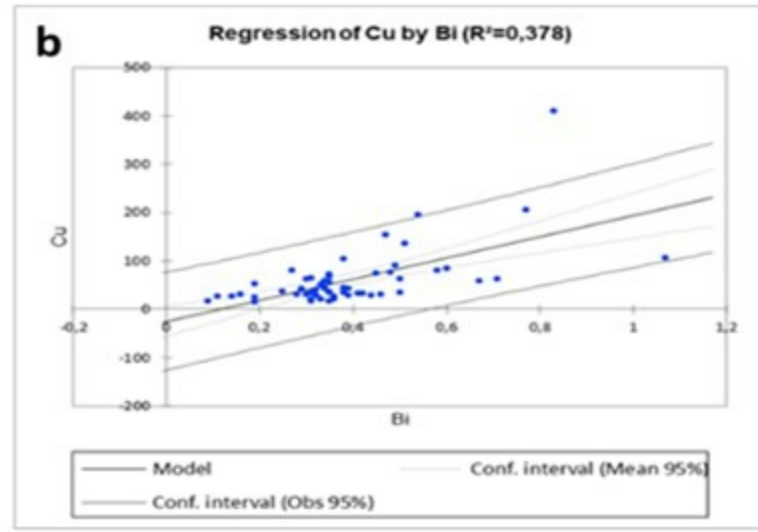
b
Regression of Cu by Bi (R²=0,378)
Cu
Bi
Model
Conf. interval (Mean 95%)
Conf. interval (Obs 95%)

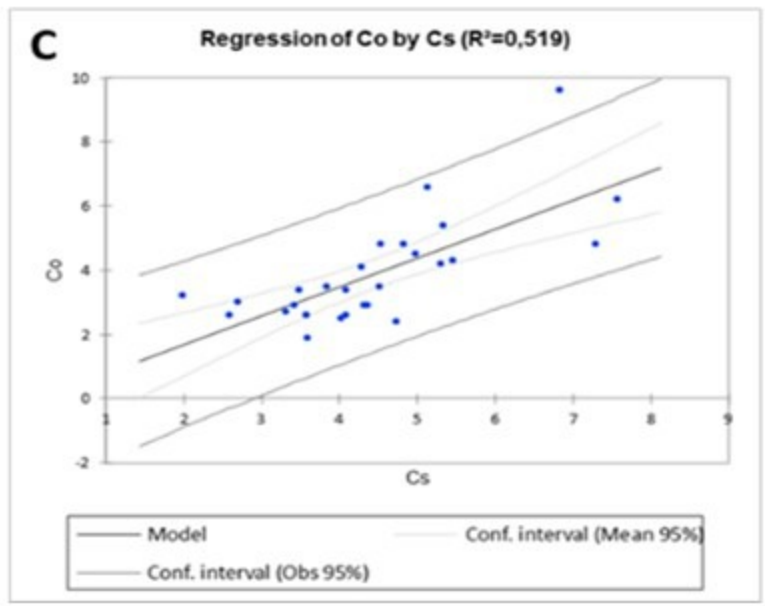
C
Regression of Co by Cs (R²=0,519)
Co
Cs
Model
Conf. interval (Mean 95%)
Conf. interval (Obs 95%)

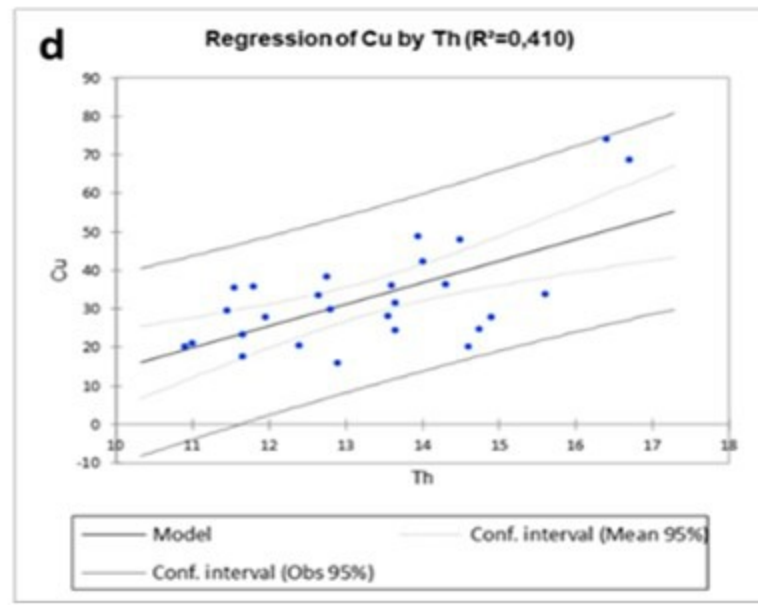
d
Regression of Cu by Th (R²=0,410)
Cu
Th
Model
Conf. interval (Mean 95%)
Conf. interval (Obs 95%)